Utilizing bimetallic catalysts to mitigate coke formation in dry reforming of methane

Jaylin Bitters Sasson[a], Tina He[b], Elizabeth Nestler[a], Sanjaya D. Senanayake[c], Jingguang G. Chen[c,d,*], Cheng Zhang[a,*]

[a] College of Liberal Arts and Sciences, Long Island University (Post), Brookville, NY, 11548
[b] Department of Molecular Biosciences, University of Texas at Austin, Austin, TX 78712
[c] Chemistry Division, Brookhaven National Laboratory, Upton, NY, 11973
[d] Department of Chemical Engineering, Columbia University, New York, NY, 10027

* Corresponding authors. E-mail addresses: jgchen@columbia.edu (Jingguang G. Chen), Cheng.Zhang@liu.edu (Cheng Zhang.)

Abstract
Dry reforming of methane (DRM) involves the conversion of carbon dioxide (CO_2) and methane (CH_4) into syngas (a mixture of hydrogen, H_2, and carbon monoxide, CO), which can then be used to produce a wide range of products by means of Fischer–Tropsch synthesis. DRM has gained much attention as a means of mitigating damage from anthropogenic greenhouse gas (GHGs) emissions to the environment and instead utilizing these gases as precursors for value-added chemicals or to synthesize sustainable fuels and chemicals. Carbon deposition or coke formation, a primary cause of catalyst deactivation, has proven to be a major challenge in the development of DRM catalysts. The use of nickel- and cobalt-based catalysts has been extensively explored for DRM for their high activity and low cost but suffer from poor stability due to coke formation that has hindered their commercialization. Numerous articles have reviewed the various aspects of catalyst deactivation and strategies for mitigation, but few has focused on the benefit of bimetallic catalysts for mitigating coke formation. Bimetallic catalysts, often improve the catalytic stability over their monometallic counterparts due to synergistic effects resulting from two metal-to-metal interactions. This review will cover DRM literature for various bimetallic catalyst systems, including the effect of supports and promoters, on the mitigation of carbonaceous deactivation.

Key Words:
Dry reforming of methane
Carbon dioxide
Bimetallic catalysts
Coke formation
Catalyst stability

Jaylin Sasson Bitters is presently a MS student at Columbia University. She received her bachelor's degree in Biology with a minor Chemistry from Long Island University (Post) in May 2021. Her research interest has focused on advanced catalysts for dry reforming of methane.

Jingguang Chen is the Thayer Lindsley Professor of Chemical Engineering at Columbia University, with a joint appointment at Brookhaven National Laboratory. His research interests include fundamental understanding of carbides, nitrides and bimetallic catalysts for applications in thermocatalysis and electrocatalysis. His research group utilizes a combination of experimental studies, in-situ characterization and density functional theory calculations.

Cheng Zhang is an Associate Professor in the Department of Chemistry at Long Island University (Post). She received her Ph.D. in Chemistry from the City University of New York in 2005. She had worked in industries for ten years before joining LIU (Post). She is the recipient of NSF-RUI, ACS-PRF and Visiting Faculty Program with Department of Energy at Brookhaven National lab. Her research focuses on the synthesis and characterization of carbon nanomaterials and catalysts for carbon dioxide, methane, and biomass conversions.

1. Introduction

The dependence on fossil fuels to meet increasing demand for energy has resulted in detrimental effects; by growing emission of greenhouse gases (GHG) such as CO_2 and CH_4 [1], major contributors to climate change and resulting increase to the global temperature. To mitigate the effects of GHG emissions, various routes for the sustainable production and consumption of fuels and chemicals have been explored; including carbon neutral and recycling strategies. Dry reforming of methane (DRM) reaction is one such strategy that has a promising application for that the simultaneous conversion of methane and carbon dioxide, to synthesis gas (syngas), H_2 and CO, which can be used as feedstocks to synthesize other important chemicals such as methanol and ammonia, as well as synthetic hydrocarbon fuels [2].

Although DRM offers important advantages for reutilization of CO_2, its large-scale application is challenged by certain critical process limitations such as high energy requirements and catalyst deactivation. Rapid carbon deposition on catalysts [3] is a major cause of poor performance and catalyst deactivation. The active sites and mechanisms involved in catalyst deactivation have been intensively reviewed [4–13], however, the focus of the current article is focused on the benefits of using bimetallic catalysts in the mitigation of coke formation.

1.1 Reaction mechanisms

The DRM reaction requires the activation of C-H and C-O bonds in methane and CO_2, respectively. In the DRM reaction, the adsorption and decomposition of CH_4 typically occur on metal active sites and the dissociative adsorption of CO_2 occurs on an oxygen vacancy site on an oxide support or at the metal/oxide interface. The activated CH_4 species form hydrogen and methyl-like species, resulting in either CH_4^* or CH_3^*, depending on the type of catalysts. [14]. The CH_x-H bond dissociation energies and rates of reaction are dependent on the surface properties of the individual catalysts [15]. Concurrently, the dissociative adsorption of CO_2 results in the formation CO and adsorbed oxygen species [16]. Direct adsorption of CO_2 on the metal particle is structure sensitive (similar to CH_4) and preferably occurs at sites with low coordination. The bonding configuration of CO_2 affects preference for the DRM reaction. In general, CO_2 shows a preference for adsorbing at the metal-support interfacial sites, which supports the general finding of small catalyst particles resulting in greater activity [16]. Following adsorption, CO_2 undergoes dissociation (to CO and O), oxidation (to CO_3), or disproportionation (reaction with gaseous CO_2 to CO and CO_3), creating reactive species to move the DRM forward upon reaction with the CH_x species [17].

Mechanistic predictions suggest that hydrogen and oxygen spillovers are the primary methods for the reaction to proceed. The spillover sites for each species are hypothesized to be most active at the catalyst/support junction. These spillovers typically occur from the metal surface to the oxide support for hydrogen, while the spillover of oxygen is from the support to the metal. The hydrogen spillover mechanism consists of several steps. In the first, molecular hydrogen is activated and dissociated on the metal catalyst (e.g., platinum, palladium, cobalt, or nickel [18]) in close contact with the substrate. The second step involves the migration of H atoms from the catalyst particles to the substrate. The last two steps involve the diffusion and recombination of H atoms on the substrate surface [19].

A key reaction step of DMR is that the oxygen species (O and OH), produced from the CO_2 dissociation, are required for the oxidation of the CH_x species on the metal sites to produce CH_xO

intermediates, which decompose to produce H_2 and CO [17,20]. Table 1 summarizes the elementary steps associated with the DMR reaction; some of the reaction steps are also illustrated in Fig. 1.

Table 1. Fundamental reaction steps on metal catalysts for the DRM process [21].

Reaction description	Reaction steps
CH_4 activation (absorption and dissociation)	$CH_4 + 2* \leftrightarrow CH_3* + H*$ $CH_4 + * \leftrightarrow CH_4*$ $CH_3* + * \leftrightarrow CH_2* + H*$ $CH_2* + * \leftrightarrow CH* + H*$ $CH* + * \leftrightarrow C* + H*$
CO_2 activation (absorption and dissociation):	$CO_2 + {}^{\#} \leftrightarrow CO_2{}^{\#}$ $CO_2{}^{\#} + H* \leftrightarrow CO\# + HO*$ $CO^{\#} \leftrightarrow CO + {}^{\#}$ $CO_2\# + * \leftrightarrow CO\# + O*$
H_2O formation:	$O* + H* \leftrightarrow * + HO*$ $HO* + H* \leftrightarrow H_2O(g) + 2*$
CO and H_2 formation:	$CH_x* + HO* \leftrightarrow CH_xO* + H*$ $CH_x* + O* \leftrightarrow CH_xO* + *$ $CH_xO* \leftrightarrow CO* + xH*$ $C* + O* \leftrightarrow CO*$ $CO* \leftrightarrow CO + *$ $2H* + * \leftrightarrow 2* + H_2$

* Indicates metal sites.
# Indicates support sites.

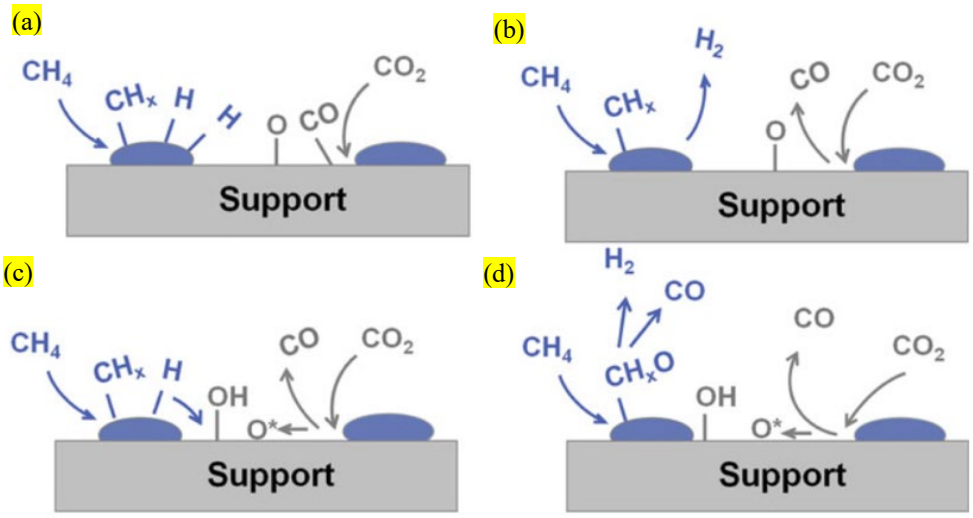

Fig 1. Representation of principal steps of DRM reaction. (a) Dissociative adsorption of methane and carbon dioxide on the metal and the metal–support junction, respectively. (b) Release of adsorbed CO and H_2 (rate-determining steps). (c) Formation of hydroxyl groups on the surface formed from hydrogen and oxygen spillover.

(d) Intermediate oxidation and desorption: oxygen or hydroxyl species on the surface oxidize the adsorbed methyl-like species resulting in either S_1–CH_xO or S_1-CO intermediates, and eventually forming CO and H_2. Reproduced from Ref. [17].

1.2 Brief summary of DRM thermodynamics

The DRM reaction is extremely endothermic and requires high operating temperatures, usually in the range of 650–1000°C to achieve the desired extent of conversion [22,23]. The Gibbs free energy of the DRM reaction decreases with temperature. According to thermodynamic analysis of DRM, a spontaneous reaction cannot occur below 640 °C [24].

The main reactions governing the DRM process are:

$CH_4 + CO_2 = 2CO + 2H_2$	(ΔH_{298K} = +247 kJ/mol)	(DRM)
$CO + H_2O = CO_2 + H_2$	(ΔH_{298K} = -41.5 kJ/mol)	(water-gas shift)

The main reactions responsible for carbon formation during DRM are:

$2CO = CO_2 + C$	(ΔH_{298K} = -171 kJ/mol)	(Boudouard reaction)
$CH_4 = C + 2H_2$	(ΔH_{298K} = 75 kJ/mol)	(methane cracking)

Wang et al. reported that CH_4 decomposition occurs at above 557 °C, while the Boudouard reaction occurs at below 700 °C. They found that carbon is formed from CH_4 decomposition or the Boudouard reaction in the temperature range of 557 to 700 °C and suggested that the optimum temperature, considering the conversion and carbon formation, is between 870 and 1040°C at the feed ratio of CO_2/CH_4 = 1:1, [25]. However, such temperatures can lead to reactor blockages and reduction in activity due to catalyst deactivation [26,27]. Moreover, during the DRM process, the reverse water gas-shift (RWGS) also occurs in parallel, resulting in higher CO_2 conversion than that of CH_4 in equilibrium leading to a H_2/CO ratio less than unity [28]. A detailed thermodynamic analysis of DRM process, including 17 possible side reactions, has been reported by Nikko and Amin [29]. Fig. 2 illustrates the typical thermodynamic equilibrium concentrations of reactants and products of DRM as a function of the reaction temperature [30].

As demonstrated by Kahle et al. for DRM operation at high temperatures (850−1000 °C) and high pressures (20 bar), methane decomposition was the main cause of coke formation; coking was found to be inhibited by H_2 rather than by water addition in the feed stream [31]. Catalyst deactivation may also occur due to thermal sintering of metal particles, a common problem of catalytic processes operated at high temperatures.

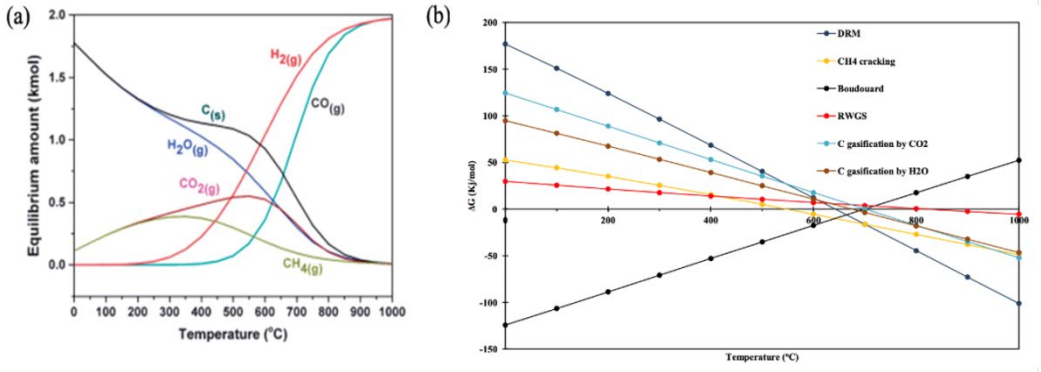

Fig 2. Thermodynamic analysis of DRM reaction: (a) equilibrium of DRM at standard atmospheric pressure from 0–1000 °C with a feed ratio of 1 CO_2: 1 CH_4 (assuming carbon formation occurs). Reproduced from Ref. [30]. (b) determination of side reaction spontaneity. Reproduced from Ref. [32].

The DRM reaction is typically performed at atmospheric pressure. This is because of an increase of coke precursors due to the promotion of methane decomposition that occurs with both increasing pressure and temperature [31]. On the other hand, a higher syngas throughput is obtained through higher pressures and therefore it is of interest to predict the performance of the reactor at these conditions [33]. Chein et al. evaluated the thermodynamic equilibrium of DRM by Gibbs free energy minimization at elevated pressures. They reported that with an increase in pressure, lower CH_4 and CO_2 conversions were obtained. Moreover, carbon and H_2O formation were found to increase with increasing pressure [34].

Traditionally, nickel-based catalysts are used for the DRM reaction due to their affordability and high activity. However, these catalysts are prone to deactivation due to carbon deposition, as well as sintering. This problem is severe in the case of DRM, where the endothermic nature of the reaction requires high operating temperatures. Precious metals such as Pt, Rh or Ru are less prone to coke formation; however, their high costs hinder the economic feasibility of the process [35]. Therefore, in order to leverage the advantageous properties associated with different metals, bimetallic catalysts have been explored for their ability to mitigate catalyst deactivation due to the synergistic effect of the two active metals.

1.3 Reaction kinetics

Soler et.al performed detailed kinetic studies of DRM over Ni–Ce/Al_2O_3 catalysts taking into account both the main reactions and the catalyst deactivation. The kinetic models included the initial reaction rate for the dry reforming, WGSR and methane decomposition reactions and Langmuir-Hinshelwood type models were employed to fit the experimental data. Among the models considered, the best fit was obtained when a residual activity was included in the model, as a result of the competition between coke formation and coke removal, with two active sites involved in the rate determining step of coke formation. Fig. 3(a) shows the relationship between calculated activity at the reactor output and coke content in the catalytic bed. The obtained parity plot is shown in Fig. 3(b), demonstrating an excellent correlation between the experimental and simulated results [36].

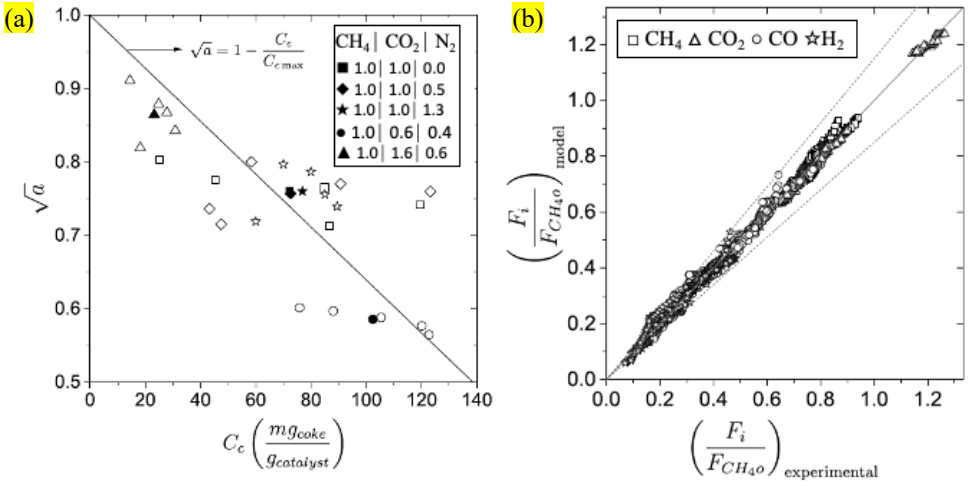

Fig. 3 (a) Relationship between catalyst activity and deposited coke content (hollow markers represent the experimental values, and filled markers represent the experimental average values). (b) Parity plot for total kinetic modelling (zero-time modelling and catalyst deactivation modelling). Reproduced from Ref. [36].

Wei and Iglesia's results of isotopic studies and forward rate measurements led to a comprehensive mechanistic picture for the CH_4-CO_2 reaction on Ni-based catalysts. They found that CH_4 reaction rates were limited solely by the C–H bond activation steps and unaffected by the identity or concentration of co-reactants. Isotopic tracer and exchange studies confirmed that C-H bond activation was the only kinetically relevant step. The results also showed that activation of CO_2 was reversible and quasi-equilibrated during CO_2 reforming reaction of CH_4. The rate of carbon formation increased with increasing Ni particle size, even though exposed Ni surface areas were lower and carbon must diffuse through larger Ni crystallites. [37].

Furthermore, Wei and Iglesia reported on the structural requirements and reaction pathways of DRM over precious metal-based catalysts (Pt, Rh, Ru, and Ir) supported on ZrO_2 or Al_2O_3. They found that reforming and decomposition rates were first-order in CH_4 concentration and independent of the concentration or identity of the co-reactants, suggesting that reaction rates were exclusively limited by C-H bond activation on metal cluster surfaces and that co-reactant activation was not kinetically relevant. The type of oxide supports influenced the metal dispersion, but not turnover rates, indicating that co-reactant activation on supports was not kinetically relevant. No detectable carbon formation was reported over the investigated precious metal catalysts. The authors suggested that even if carbon species were formed on the catalyst the carbon removal rate should be higher than the carbon formation rate, thus preventing net carbon accumulation on the catalyst surface and consequently the stable catalytic performance [38–40].

1.4 Classification of bi-metallic catalysts

Several approaches have been investigated in order to overcome catalyst deactivation. One solution is to create a bimetallic catalyst, where a precious or non-precious metal is added to another primary metal. This approach can potentially mitigate the deactivation of non-precious catalysts caused by excessive coke formation and sintering. The addition of small amounts of precious metals (Rh, Ru, Ir, Pt, Pd, Au) or non-precious metals (Ni, Co, Cu, Fe, Sn, etc.) to conventionally non-precious metal catalysts typically increases metal dispersion, decreases the particle size and thus retains a good catalytic activity and stability [41–47]. For example, in a bimetallic Ni-Co catalyst, hydrogen spillover from Ni to Co prevents its oxidation, while the high oxygen affinity of Co contributes to C* oxidation by the reverse Boudouard reaction for removing coking [48–50]. In a Ni-Fe catalyst, the redox ability of Fe allows it to react with surface carbon species, thus reducing coking [50]. Promotion with precious metals improves reducibility. For example, with Ni-Pt, reduction is facilitated by the initial reduction of adjacent Ni and Pt atoms forming an alloy, then reduction of the remaining Ni into a separate phase facilitated by H_2 spillover. Tomishige et.al noted that the reducibility of the catalyst determined the activity and resistance to coking [51–53]. In a Rh-Ni catalyst, the elimination of coke deposition on Rh-promoted catalysts was attributed to the formation of Rh-Ni clusters having a Ni covered surface, thus enhancing the dispersion of the nickel particles and favoring the formation of more reactive intermediate carbonaceous species [54–56]. Some promoters occupy the steps sites where carbon nucleates, such as Sn or Au. For example, Sn alloying with Ni was observed to have a positive effect towards increased catalyst stability by inhibition of carbon nucleation on the active Ni step sites [57]. Several studies have highlighted the importance of maintaining high dispersion and

surface area, in addition to small metal particle size in order to achieve high catalytic activity, stability and avoid excessive carbon formation [58–61]. This enhancement of the catalytic performance and coke resistance is achieved by increasing the dispersion of the active metal particles and decreasing their size, enhancement of the catalyst reducibility, decreasing the rate of coke formation, altering the type of coke deposited on the catalyst surface, in addition to creating a synergic effect between the metals involved [60–64].

The synergistic effects of bimetallic catalysts for controlling and improving the DRM activity, selectivity and stability have been extensively discussed in a recent review [11]. The focus of the current review is on the reaction mechanisms and recent advancement in utilizing bimetallic catalysts to mitigate coke formation in DRM.

2. Catalyst deactivation from coke formation

During the transformation of organic compounds over acid and over bifunctional metal-acid catalysts, carbonaceous deposits are formed. The formation of these non-desorbing products, also known as coke, is a major cause of catalyst deactivation in industrial processes [65]. The deactivation of the catalysts generally results from pore blockages or poison of the active sites. Although the deactivation caused by coking is often reversible, typically removed by oxidation, regeneration can be detrimental due to numerous secondary effects under the severe conditions of coke removal such as high temperature, presence of water, etc.

The chemical composition of coke depends on several factors under which the reaction is taking place, such as the type of catalyst, the nature of the feed gas [66] and the conditions under which the reaction is performed, most importantly, temperature. At above 350°C, the coke components are typically polyaromatic and their formation involves hydrogen transfer (acid catalysts) and dehydrogenation (bifunctional catalysts) steps in addition to condensation and rearrangement steps. Furthermore, the composition of the carbonaceous deposits is also significantly dependent upon the nature of the catalytic active sites, which ultimately determines the reaction steps that can be catalyzed. Furthermore, the size of the coke molecules can be limited by the size of the pores of in porous materials, known as the confinement effect [67]. Pore size is an important parameter that impacts not only the physico-chemical properties of porous material but also the properties of chemical species inside their pores and can strongly affect diffusion, phase transformation, catalytic properties, etc. [68]. In using support materials with the proper pore size, active metal sites can be maintained in a confined structure, thus preventing the formation of multiple aromatic carbon rings on the surface of the catalyst. Furthermore, maintaining a low number of metal atoms within a microporous structure also potentially enables the prevention of agglomeration of metal clusters at high temperatures.

On microporous catalysts, the retention of polyaromatic carbon species results from steric blockage within the micropores. Due to the high temperatures needed for the DRM reaction [69], the cleavage of the C-H bonds in CH_4 results in carbon deposition on the catalysts [70]. The two primary causes of carbon deposition and coking are the presence of side reactions, namely CH_4 cracking (decomposition) and the CO disproportionation (Boudouard reaction) [71,72]. Typically, carbon is a product of CO disproportionation whereas coke is formed during the decomposition or condensation of hydrocarbons, such as CH_4 [73,74]. Methane decomposition typically occurs at

temperatures above 557°C, and the Boudouard reaction at temperatures below 700°C. Thus, maximum carbon deposition is typically reported in the temperature range 557–700 °C [75].

Catalyst deactivation can result from various physico-chemical phenomena, namely metal sintering, metallic phase oxidation, thermal degradation of the support, and most commonly, carbonaceous deposition, or coking [76]. In DRM, coke deposition and thus catalyst deactivation can occur via several routes, as shown in Fig. 4. One possible outcome is that carbon accumulated on the catalyst may chemisorb strongly as a monolayer or physically adsorb in multilayers, blocking access of reactants to the active metal sites. Alternatively, the accumulated carbon may totally encapsulate a metal particle, deactivating that particle entirely. Carbon on the surface may plug micro- and mesopores restricting access of reactants to active sites inside these pores. In extreme cases, strong carbon filaments may build up in pores leading to stressing and fracturing of the support material, ultimately causing the disintegration of catalyst pellets and plugging of reactor [77,78]. The different possible outcomes for the catalyst deactivation are influenced by the forms of coke present on the surface, which can vary from high molecular weight hydrocarbons such as condensed polyaromatics to carbons such as graphite, depending upon the conditions under which the coke was formed and aged [73].

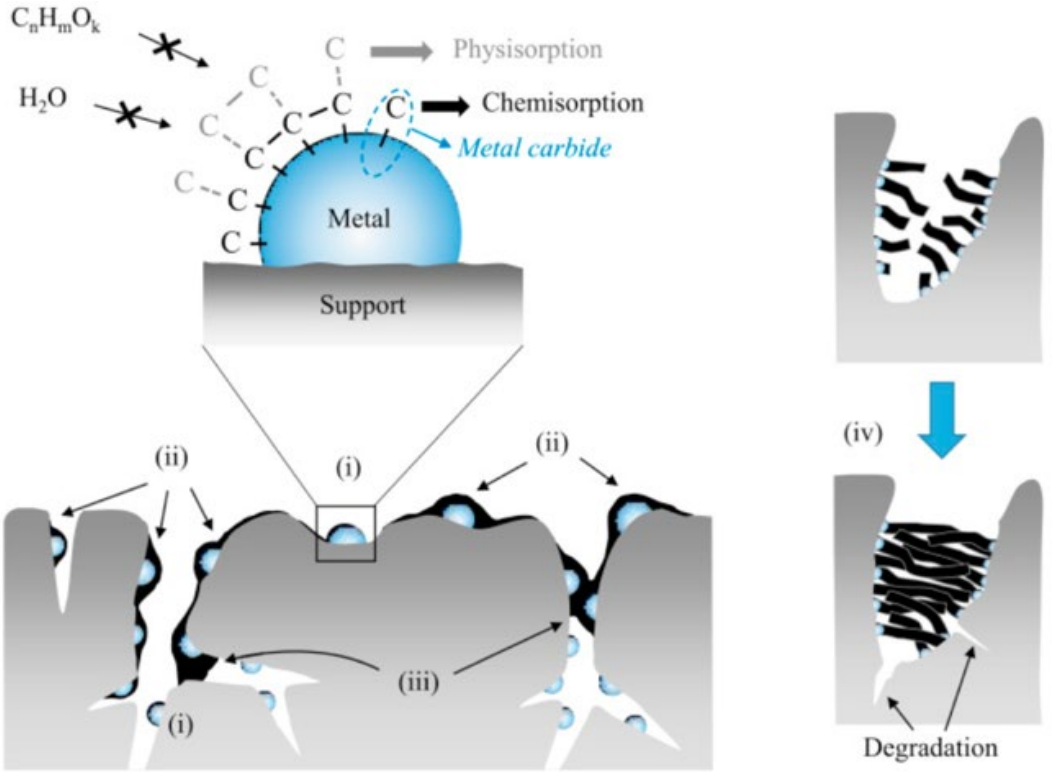

Fig 4. Possible routes of deactivation due to coke deposition on metal catalysts: (i) blockage of active sites due to accumulation; (ii) carbonaceous encapsulation of metal particle leading to its deactivation; (iii) plugging of pores on surfaces causing restricted access of active sites to reactants; (iv) stressing and fracturing of support material resulting in disintegration of catalyst pellets due to build-up of strong carbon filaments. Reproduced from Ref. [76].

Carbon deposits can take on three main forms [79]: (i) pyrolytic coke from cracking of hydrocarbons above 600°C, (ii) encapsulating hydrocarbon films formed by polymerization at less

than 500°C, and (iii) whisker carbon formed at temperatures greater than 450°C [80–82]. At low temperatures (< 500 °C), adsorbed hydrocarbons may accumulate on the surface of the catalyst and progressively polymerize into an encapsulating film, which results in the blocking and deactivating of the metal sites. At high temperatures (>600 °C), thermal cracking of hydrocarbons can lead to the formation of pyrolytic coke that may encapsulate and deactivate the catalyst particle. At temperatures greater than 450 °C, the dominant product of carbon formation is whisker carbon [83]. Whisker carbon typically grows as a filamentous carbon with the metal at the top as shown in Fig. 5a and 5b. The mechanism of whisker growth has been studied by many authors [84–87]. More recent studies by Rostrup-Nielsen etc. proposed as illustrated in Fig 5c that the atomic step sites on the metal surface play a significant role in the nucleation and growth of graphene layers on the Ni surface [88–91]. DFT calculations show that dissociative methane adsorption is facilitated at the step edges and that C atoms adsorb preferentially at the step sites. The transport of C atoms from the free Ni surface to sites at the graphene-Ni interface consists of three steps: the breaking of the C-H bond to the Ni-step, incorporation under the graphene sheet, and diffusion at the graphene-Ni interface. Fig. 6a-c shows the time-lapsed HRTEM image series at the whisker-Ni interface acquired in situ during whisker growth [88]. The images reveal that mono-atomic step-edges form spontaneously and assist the growth of additional graphene layers at the interface. The step sites bond to carbon more strongly than on the close packed Ni(111) facets, suggesting that the step sites may be the nucleation center for carbon growth. The HRTEM observations clearly pointed to a surface transport of the metal atoms from the step sites to the free metal surface (Fig. 5c) [88–91]. The whisker type carbon does not directly deactivate the surface but rather causes a breakdown of the catalyst by pore plugging [92–94]. Table 2 shows the different types of carbon and coke that vary in morphology and reactivity. Different carbon species can form on the surface of the catalyst based on the thermodynamic conditions and catalyst properties, and therefore there is no unique description for carbon species on a catalyst.

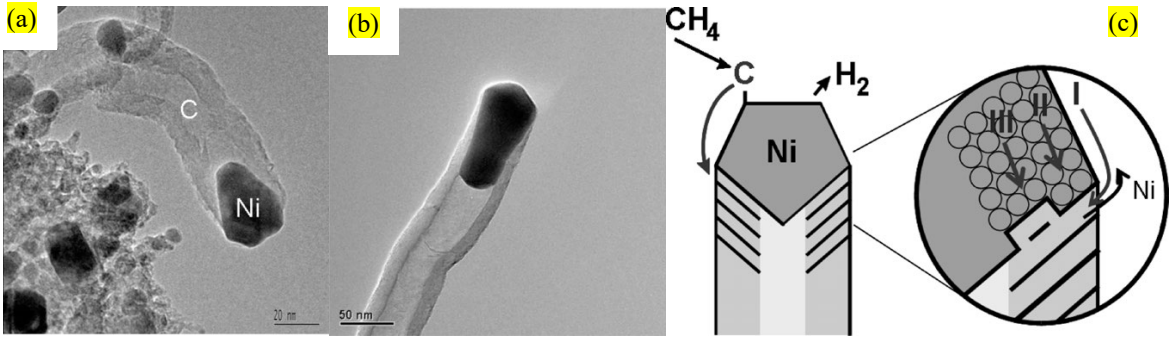

Fig. 5. (a) and (b) HRTEM images of carbon whiskers. (c) Illustration of the whisker growth mechanism based on step-site mediated graphene growth and transport processes confined to the surface region. Reproduced from Ref. [88].

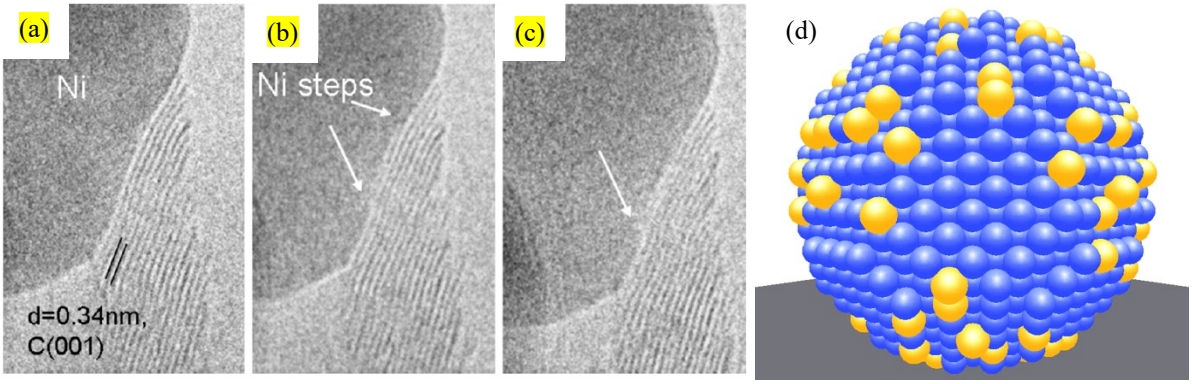

Fig. 6 (a-c) Snapshot of a whisker growth. HREM. The step sites move as the graphite plane grows [88]. (d) Step blocking for Ni-Au surface alloy. Reproduced from Ref. [98].

Table 2. Typical carbon species on nickel catalysts for DRM. Reproduced from Ref. [73].

Attribute	Encapsulating film	Whisker-like	Pyrolytic carbon
Formation	Slow polymerization of C_nH_m radicals on Ni surface, into encapsulating film	Diffusion of C through Ni crystal, nucleation and whisker growth with Ni crystal at top	Thermal cracking of hydrocarbon; deposition of C precursors on catalyst
Effects	Progressive deactivation	No deactivation of Ni surface. Breakdown of catalyst and increasing ΔP	Encapsulation of catalyst particle; deactivation and increasing ΔP
Temp. range, ºC	<500	>450	>600
Critical parameters	Low temperature, low H_2O/C_nH_m, low H_2/C_nH_m, aromatic feed	High temperature, low H_2O/C_nH_m, no enhanced H_2O adsorption, low activity, aromatic feed	High temperature, high void fraction, low H_2O/C_nH_m, high pressure, acidic catalyst

There are five distinct types of carbon deposits from CO and hydrocarbons, specifically on the surface of nickel catalysts. The surface carbon species most commonly deposited during the DRM process include C_α, C_β, C_γ, C_v, and C_c. The smallest coke classified by Argyle et al. [77] is an alpha coke, C_α, presented in the form of an atomic carbon. C_α is the initial reactant to the formation of all other types of coke. The initial step of coke formation, dimerization, is the first condensation step of C_α and leads to the formation amorphous carbon (the most reactive form), composed of carbon atoms adsorbed and bound to metallic centers [30], which results in the formation of larger coke [95]. An example of this was provided by Arora and Prasad, who elaborated on this process by highlighting the dissociation of CO on metals at the catalyst surface forming C_α, which reacted to produce C_β, polymeric carbon, that further reacted to form C_γ, C_v, and C_c [75]. The oxidation temperature of polymeric carbon increases with decreasing H:C ratio. Furthermore, C_β is able to be oxidized under mild conditions and do not result in blockage of the active sites. The graphitic

form of carbon, C_c, consists of six-carbon ring compounds (polynuclear aromatics) and is the least reactive. Graphitic, C_c, and filamentous, C_v, forms of carbon require high temperatures for oxidation and can block the active sites inducing deactivation [30].

It is important to note that not all forms of carbon negatively impact catalytic activity and various critical parameters must be considered to determine the severity of the effect of the carbon species on the catalyst. These points are summarized in Fig. 7 and Table 3, which provide details about these different forms of carbon with their respective temperature ranges. Under the conditions of the DRM reaction (700-850 °C), C_v and C_c are typically the forms of coke observed on the catalyst surface. The C_v, or whisker carbons, are graphitic and tubular in shape, form due to the presence of a dissolved carbon concentration gradient. The C_c, graphitic films, diffuse across the metal particle surface and develop into ordered graphite layers parallel to the metal-carbon interface [83].

Table 3. Various carbon species formed by decomposition of CO on nickel. Reproduced from Ref. [73].

Structural type	Designation	Temp. formed, ºC	Peak temp. for reaction with H_2, ºC
1. Adsorbed, atomic (surface carbide)	C_α	200-400	200
2. Polymeric, amorphous films or filaments	C_β	250-500	400
3. Vermicular filaments, fibers and/or whiskers	C_v	300-1000	400-600
4. Nickel carbide (bulk)	C_γ	150-250	275
5. Graphitic (crystalline) platelets or films	C_c	500-550	550-850

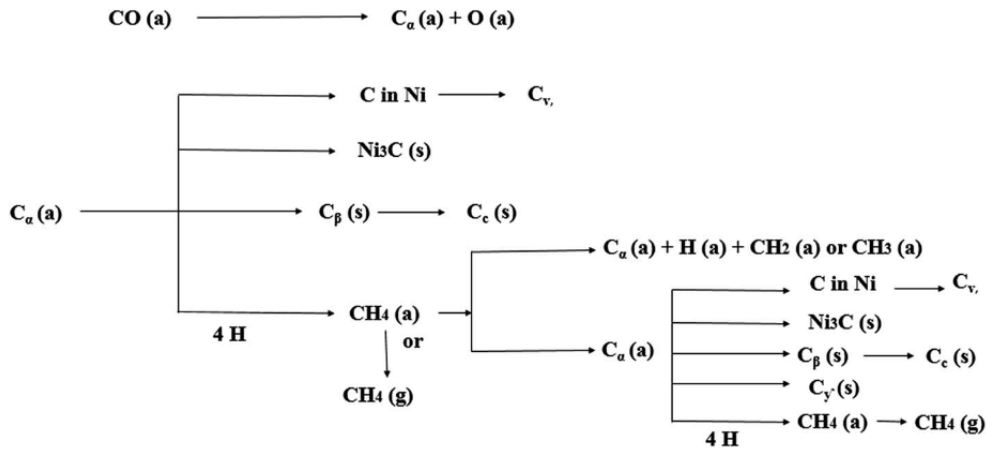

Fig 7. Routes of carbon formation on catalytic surface, depending on reaction conditions. Reproduced from Ref. [75].

Presently, the most commonly used catalysts for the DRM reaction consist of supported nickel-based catalysts supported on aluminum oxides. However, these catalysts also catalyze carbon formation reactions resulting in loss of catalytic activity [96]. The most notorious type of carbon

deposition on nickel catalysts is whisker carbon due to solubility of carbon in the non-precious metals and its diffusion through the metal lattice [70]. Because of its high strength and ability to cause pore damage and detachment of active metal particles from the support, whisker carbon is often considered to be the most detrimental form of carbon that can grow on the catalyst surface [97]. The nucleation of carbon can be eliminated or retarded by blockage of the step sites. As reported by Rostrup-Nielsen etc., additives like potassium, sulfur, and gold preferentially bind to the step sites of Ni, suggesting that the promotion effect by these additives in terms of suppression of graphite formation is due to the blocking of the step sites (Fig. 6d). This is confirmed by DFT calculations showing a higher activation barrier for decomposition of methane on the Ni-Au surface alloy [90,98–100]. Similarly, in the Sn/Ni surface alloys, Sn-induced increase in the diffusion barriers suggests that C and O atom diffusion is kinetically important for the respective C-C and C-O bond formation over Sn/Ni, leading to the suppression of carbon growth by Sn alloying of Ni [100]. The DFT results also revealed that there is a favorable thermodynamic driving force for Sn to displace Ni atoms from the step-edge sites. In these configurations the Sn step-edge atoms effectively repel C atoms from the low-coordinated step sites. Since low-coordinated step sites have been proposed to play a role in the nucleation and growth of carbon deposits over Ni, this arrangement of Sn atoms further lowers the propensity of the alloy to form carbon deposits [100–102].

As a strategy to minimize, or ideally inhibit, carbon formation, utilization of two active metals to create an interstitial alloy has been extensively explored. By taking advantage of the synergistic interaction between the two metals, researchers hope to use the alloy catalysts to mitigate carbon deposition and catalyst deactivation, as summarized in the following section.

3. Utilization of bimetallic catalysts to mitigate carbon deposition

Supported metals have long been investigated as catalysts for DRM partially due to their ability to overlap d-orbitals with the π electrons of carbon monoxide and carbon dioxide. Generally, single metal catalysts suffer from a lack of activity, selectivity, or accelerated deactivation. Combinations of metals have been explored to harness the best properties of the individual elements, while minimizing each of their drawbacks [103]. The three primary electronic mechanisms for modification of the chemical properties of these bimetallic surfaces are the “strain effect”, “ligand effect” and “ensemble effect”. The strain effect refers alterations in the chemisorption properties of the active metals due to the changes in bond lengths of the material as a result of differences in the lattice constants of the components [104]. The average bond lengths between the metal atoms in the bimetallic catalysts are typically different than those in the parent metals, resulting in changes due to strain that leads to alterations in the chemisorption properties. The ligand effect refers to the modification of the surface electronic structure of the heterometallic bonding interactions, thus changing the surface chemical properties of the catalyst [105–107], resulting in a reduced binding energy of carbon to the catalyst surface and thus reduced coking. The ensemble effect typically describes the availability of an ensemble of the same metals, which is altered due to the mix of the two metal components and consequently change the local chemisorption properties. The synergetic effects of bimetallic helps to enhance dispersion as well as to enhance DRM performance. Several bimetallic combinations have been extensively investigated for their influence over catalytic activity with the goal of minimizing carbonaceous deposit and thus, deactivation of the catalyst [108,109]. Ni-Co bimetallic catalysts have been widely explored as potential catalysts for use in DRM due to their advantages in activity and costs. Ni and Co easily form alloyed nanoparticles, and thus exhibiting a synergistic effect on one another. The main

drawback of monometallic Co and Ni catalysts is their deactivation by coke deposition as the reaction progresses. In this section, we use selected examples to demonstrate the trends in the utilization of bimetallic catalysts to mitigate coke formation; Table 4 summarizes some of the main observations of the studies reviewed.

Table 4. Representative bimetallic DRM catalysts

Bimetallic catalyst	CH_4 Conversion (%)	CO_2 conversion (%)	H_2/CO ratio	Carbon deposition	Reference
Co-Ni/CeO_2 (Co 3.75 wt%, Ni 3.75 wt%)	97% (800 °C)	~96% (800 °C)	~1 (>700 °C)	6 wt % of deposited amorphous carbon (22 h)	[116]
Ni_9Co_1/SBA-15	59% (700 °C)	71% (700 °C)	~0.96 (700 °C)	n.d. (50 h)	[122]
4Ni-1Co/CF-La_2O_3	88% (750 ◦C)	83% (750 ◦C)	1.1	n.d. (10 h)	[14]
Ni-Co-Al-Mg-O	91.4% (750 ◦C)	---	~1 (750 ◦C)	Very low; 0.00204 $g_c/g_{cat}{}^{-h}$ (28 h)	[26]
5% Ni–5% Co/Al_2O_3	16.5% (600 ◦C)	35 (600 ◦C)	0.85 (600 ◦C)	21.2 wt% (4 h)	[124]
5% Ni–10% Co/Al_2O_3	67% (700 °C)	71% (700 °C)	~1 (700 °C)	---	[111]
Ni-Co/HAP SIWI	73% (750 °C)	79% (750 °C)	0.88 (750 °C)	13% (50 h)	[112]
NiCo/MAl	33% (750 °C)	47% (750 °C)	0.96 (750 °C)	(7 h)	[159]
4.5Ni0.5Co/SBA-15	39.1% (800 °C)	65% (800 °C)	0.63 (800 °C)	46.8% (30 h)	[123]
4Ni-1Co@SBA-15	75% (750 °C)	90% (750 °C)	1.24	Very low filamentous carbon (4 h)	[119]
$NiCo_{2(4.6)}/Mg_{0.9}$(Al)O	43% (800 °C)	---	0.75 (800 °C)	Very low coke formation rate (20 h)	[153]
1Ni8Co/Al_2O_3	73% (700 °C)	80 (700 °C)	--	Coking amount = 20 mg/g_{cat} (after 6 h)	[27]
Co_5Ni_5/ZrO2	70% (750 °C)	83% (750 °C)	0.9 (750 °C)	0.17% (20 h)	[120]
0.8Co–Ni/CeO_2	77% (800 °C)	80% (800 °C)	0.92 (800 °C)	Less than monometallic (10 h)	[113]
$Ni_{0.8}Co_{0.2}$/H-ZrO_2	92.5% (700 °C)	90% (700 °C)	0.78 (700 °C)	Lower than monometallic (80 h)	[125]
Ni–Co/γ-Al_2O_3 catalyst + 0.25 wt% Sr	85.8% (700 °C)	84.2% (700 °C)	---	9.1 wt% (7.5 h)	[110]
$In_{0.5}Ni@SiO_2$	90% (800 °C)	97% (800 °C)	1/1 (800 °C)	n.d. (20 h)	[128]
Ni-Fe/Mg(Al)O	97% (800 °C)	99% (800 °C)	0.85 (800 °C)	<3 wt% (25 h)	[129]
12%Ni-4%W/Al_2O_3-MgO	95% (800 °C)	95.6% (800 °C)	0.95 (800 °C)	Less than monometallic (6 h)	[130]
$NiSn_{0.2}$/Al	30% (700 °C)	65% (700 °C)	0.9 (700 °C)	Decreased rate of carbon formation (20 h)	[131]
Ni-Mo/MgO	~99% (800 °C)	~100% (800 °C)	1 (800 °C)	n.d (850 h)	[133]
20Mo10Ni/Al_2O_3	30 % (800 °C)	88% (800 °C)	0.8 (800 °C)	Less than monometallic	[134]
10 wt% Ni/$MgAl_2O_4$	84.7% (750 °C)	92.6 % (750 °C)	0.98 (750 °C)	8.6 wt% (10 h)	[135]
25Ni-5Ce-Al_2O_3	70% (700 °C)	78% (700 °C)	0.82 (700 °C)	Less than monometallic (5 h)	[138]

10 wt%Ni/5 wt%CeO$_2$/Al$_2$O$_3$	~83% (800 °C)	~87% (800 °C)	~0.9 (800 °C)	Less than monometallic (18 h)	[140]
10%Ni/3%CeO$_2$–3%La$_2$O$_3$–γ-Al$_2$O$_3$	77.27% (800 °C)	97.05 (800 °C)	1.09 (800 °C)	0.0349g/0.2 g$_{cat}$ (8 h)	[139]
2Ni–1Zr/MCM-41	90% (750 °C)	---	1.1 (750 °C)	Minimum % of inert carbon (72h)	[141]
Ni$_{10}$-V-MgAl	90% (700 °C)	94% (700 °C)	0.91 (700 °C)	Better anti coking than monometallic (12% wt loss); (80 h)	[143]
0.5Mo-1Ni/SBA-15	94% (800 °C)	---	0.96 (800 °C)	Carbon deposition rate =0.00198 $g_c \cdot g_{cat}^{-1} \cdot h^{-1}$ (250 h)	[136]
8 wt%Ni 8 wt%Mo/Al$_2$O$_3$	~97% (800 °C)	~95% (800 °C)	0.94 (800 °C)	Carbon formation rate, (mmol C/mol CH$_4$ reacted) = 0.21	[31]
NiPd/SiO$_2$-OA	65% (700 °C)	76% (700 °C)	~0.9 (700 °C)	7.9 wt% (25 h)	[149]
7.5%(Ni$_{0.8}$Pd$_{0.2}$)/ZrO$_2$-La$_2$O$_3$	~78% (700 °C)	~73% (700 °C)	~0.96 (700 °C)	---	[150]
2 wt% Pt–2 wt% Ni/CeO$_2$	85% (800 °C)	90% (800 °C)	---	0.108 μmol (24h)	[151]
5%Ni-0.1%Pt/MgO	~80% (700 °C)	~85% (700 °C)	---	n.d. (50 h)	[152]
Ru$^{0.1\%}$–Ni$^{5.0\%}$/MgAlO$_x$	94% (800 °C)	97% (800 °C)	1 (800 °C)	7 wt % - low coking capacity (50h)	[154]
Ni-Ru/Ce-KIT-6	97% (800 °C)	95% (800 °C)	~0.93 (800 °C)	~52-55% (but no deactivation observed) (12 h)	[155]
15 wt% Ni–0.5 wt% Ru/MgO/Al$_2$O$_3$	30% (650 °C)	40% (650 °C)	0.8 (650 °C)	Increased resistance to carbon deposition	[159]
5Co-2Ce/ZrO	48.9% (650 °C)	61.1% (650 °C)	0.81 (650 °C)	2.0 wt% (6 h)	[161]
5%Co-2%Ce/ZnO	73% (700 °C)	83% (700 °C)	0.59 (700 °C)	Lowest carbon deposition observed (600 °C)	[162]
Ru-Co@SiO$_2$-P	74.4% (700 °C)	84.7% (700 °C)	0.98 (700 °C)	Carbon deposition rate=0.5 $mg_{coke}\ g_{cat}^{-1}\ h^{-1}$ (10 h)	[163]
PtMo/Ni/Al$_2$O$_3$-CeO$_2$	72% (700 °C)	78% (700 °C)	0.87 (700 °C)	Less than monometallic promoted (10 h)	[167]
Co$_3$Mo$_3$N	~95% (800 °C)	~98% (800 °C)	~0.9 (800 °C)	More resistant to oxidation than monometallic (50 h)	[168]
Rh$_{0.5}$Co$_{12}$/SBA-15	~100% (800 °C)	~91% (800 °C)	>1 (800 °C)	Less C_γ than and higher C_α than monometallic Co	[164]
Co-Ru/TiO$_2$ (Ru = 0.05)	14.2% (750 °C)	28.6% (750 °C)	---	n.d. (24 h)	[166]

3.1 Ni-Co bimetallic catalysts

Ni-Co bimetallic catalysts have been widely explored as potential catalysts for use in DRM due to their advantages in activity and costs. Ni and Co easily form alloyed nanoparticles, and thus exhibiting a synergistic effect on one another. The main drawback of monometallic Co and Ni catalysts is their deactivation by coke deposition as the reaction progresses. Studies have shown that the combination of Ni and Co catalysts is able to reduce carbon deposition in CO methanation, partial oxidation of methane to synthesis gas, and steam or dry reforming of methane [110]. The suppression of carbon deposition by the addition of Co to a Ni catalyst for CO methanation is likely due to an enhancement of the hydrogenation of atomic carbon and/or inhibition of the formation of metal carbide species. The adsorption strength of CO_2 and CH_4 of the catalyst decreases with the increasing size of coke due to an increased steric hindrance of larger coke when accumulated. When Siang et al. performed Raman spectroscopy analysis of spent bimetallic 5%Ni-10%Co/Al_2O_3 catalysts to study the type of carbonaceous deposition on catalyst surface, as well as SEM microscopy for morphological analysis of the used catalyst, they observed the existence of both whisker-like and graphitic carbon, with a substantially greater percentage of the whisker-like species. The nano-whisker carbon, reportedly not prone to rapid catalyst deterioration since it is highly reactive and readily eliminated from catalyst surface by CO_2 reactant via reverse-Boudouard reaction, served to explain why the 5%Ni-10%Co/Al_2O_3 catalyst did not experience catalyst deactivation over the 4 h period on stream due to the carbon deposition [111]. Similarly, when evaluating Co-Ni catalysts, Phan and coworkers did not observe the presence of amorphous carbon or core-shell carbon, primary causes of causes the catalytic deactivation in DRM reaction, both of which entirely encapsulate the metal particles and thereby completely deactivate them. The presence of cobalt in the nickel catalysts promotes the adsorption of surface oxygen and enhances carbon removal, thus making it more stable overall [112]. In their evaluation of monometallic Ni and Co-Ni bimetallic catalyst, Turap et al. reported that although carbon deposition occurred on both catalysts, the deposited carbon on bimetallic Co-Ni was reduced and more easily eliminated than on monometallic Ni [113]. Zhang et al. reported that the formation of Ni-Co alloy on the catalyst surface was confirmed from the shift of Ni and Co binding energy, resulting from the near-distance interaction between the two metal atoms [114]. This shift in the binding energy as a result of the bimetallic was further explained by Saelee and coworkers in their analysis of the surface behavior of coke on the surface of NiCo and Ni. Their computational investigation revealed that NiCo exhibited weak adsorption strength at all sizes of coke, shown in Fig. 8, suggesting that a weak bond would form if the alpha coke accumulated on such surfaces. Furthermore, if the coke condensation proceeded to form a larger coke, the binding strength of such coke would still be weak suggesting the coke-resistant property of the NiCo bimetallic. The adsorption energy of various coke adsorbed on Ni and NiCo surfaces are compared in Fig. 8. They also found that the weak binding strength of coke found in all NiCo surfaces suggested that Co in Ni-Co bimetallics served a promotional role and could weaken the interactions between the Ni and C atoms. This was beneficial for the Ni active site since the site blockage is less likely to occur, increasing available sites for the main reaction [96].

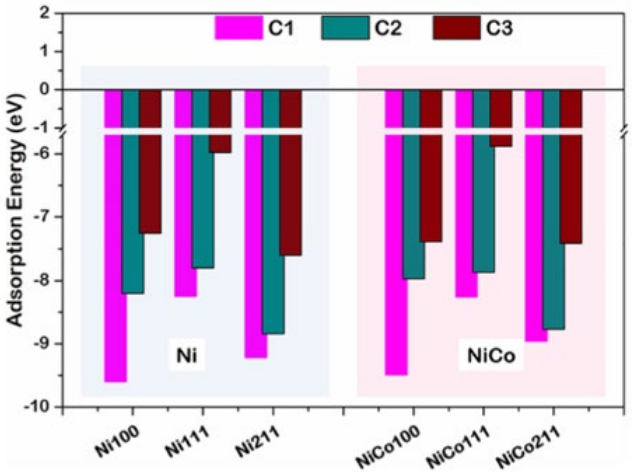

Fig 8. Adsorption energies of coke in forms of alpha and beta carbon as 1-atom (denoted as C1), 2-atom (denoted as C2), and 3-atom carbon (denoted as C3) adsorbed on the surface of Ni and NiCo, where the binding strength of coke are determined denoted as $E_{ads.}$ Reproduced from Ref. [96].

While the carbon adsorption strength provides the information of the most stable adsorption site, the energy needed for C atom diffusion is an essential parameter in understanding the propagation of coking, as well as how easily the coke can be removed from the catalyst, since it is an initial step toward coke formation. Saelee et al. found that the presence of Co in the NiCo surfaces displayed an increase in coke mobility, considered to be beneficial since easy diffusion of coke on the surface would increase the chance of coke encountering the coke-removing species, i.e., H or O for hydrogenation and oxidation of coke, respectively. They concluded that the charge transfer in α-coke coupled with the higher coke adsorption on the Ni and NiCo surfaces was an indication of a high coke-resistant property of the bimetallic NiCo surface [96].

The formation of an alloy can lead to an enhancement in specific properties upon alloying due to synergistic effects, resulting in the rich diversity of compositions, structures, and properties of metallic alloys [115]. In literature, extensive investigations of combinations between Ni and Co have been carried out for DRM. The alloying of the non-precious metals Co and Ni is utilized for their high affinity for CO_2 and high activity for CH_4 decomposition, respectively. Luisetto et al. studied MDR over Ni-Co/CeO_2 synthesized via a surfactant-assisted co-precipitation method and found that bimetallic catalysts attained superior catalytic activity (CH_4 Conv. = 97.0% at 800°C) as compared to that of the monometallic counterparts. Furthermore, the addition of Co to the Ni-based catalyst showed substantially higher resistance to carbon deposition, elucidating the effectiveness of the addition of Co in the prevention of carbon deposition [116].

Fan et al. compared the methane conversion rates under Ni/MgO-ZrO_2, Co/MgO-ZrO_2 and Ni-Co/MgO-ZrO_2. They reported that the bimetallic Ni-Co catalyst achieved the highest methane conversion rate of 80%, as compared to the monometallic Ni and Co catalysts, at 70% and 71%, respectively. The increase in the catalytic activity of the bimetallic catalyst compared to the monometallic ones was attributed to the synergic effect of Ni and Co, in addition to better metal dispersion and smaller particle size [117]. According to Takanabe et al., the formation of Co-Ni alloy was able to improve the reforming activity, especially C-H bond activation, on the metallic surface, as well as to aid in avoiding undesirable metal oxidation [118]. It has also been reported

that incorporation of Co into Ni catalysts inhibits the agglomeration of the nickel particles due to the formation of Ni-Co alloy and leads to an increased dispersion of the Ni particles [119]. AlSabban, et al. evaluated monometallic Co and Ni and bimetallic CoNi at various Co/Ni ratios. DFT calculations of their findings showed that the heat of oxygen adsorption increased monotonically with increasing Co content in CoNi alloy. The CoNi alloy for DRM could balance CH_4 and CO_2 activation kinetically, preventing both carbon deposition and metal oxidation, as shown in Fig. 9 [120]. Adjusting the composition of the active metals (Co and Ni) could kinetically control the elementary steps, namely the formation of carbon species and its removal by oxygen species during the DRM reaction [121].

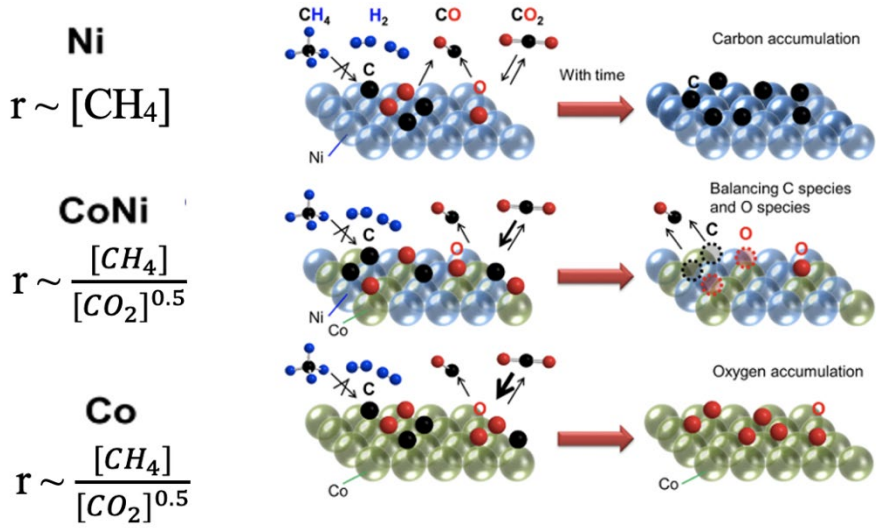

Fig 9. Schematic depicting the kinetics for the reactive surfaces for Ni, CoNi, and CO during the DRM reaction. Reproduced from Ref. [69].

The ratio of Co:Ni selected for DRM catalysts has a strong impact on the activity and stability of the catalyst. Deactivation would occur due to oxidation of the metals if the Co loading is too high, whereas deactivation could be caused by coking if the Ni loading is too high [75]. Zhang et al. found that variation in Ni-Co content in catalyst could influence the severity of carbon deposition. The lower loading bimetallic catalysts, 0.04Ni0.05Co and 0.02Ni0.03Co, completely eliminated carbon deposition due to the absence of larger metal particles (>10 nm). They reported that small metal particles were crucial to the suppression of carbon deposition [114]. Co-Ni alloys supported on CeO_2 were evaluated by Turap et al. and found to have an optimal molar Co/Ni ratio of 0.8 for the most active and stable catalysts, as well as the lowest deactivation. The Co-promoted adsorption of surface oxygen enhances carbon removal, making it more stable [119]. Xin et al. evaluated the performance of Ni-Co/SBA-15 bimetallic catalysts and found that both activity and stability decreased in the sequence of Ni_9Co_1/SBA-15 > Ni_6Co_4/SBA-15 > Ni_8Co_2/SBA-15 > Ni_{10}/SBA-15. Low Co/Ni ratio had the highest activity and stability in terms of coke- and sintering-resistance, noting that the Co/Ni mass ratio had a direct effect on metal particle size [122]. Takanabe et al. reported that, for bimetallic TiO_2 supported NiCo catalysts, an increase of the carbon deposit was observed with the Ni content [121]. This was also reported by Wu et al. after evaluating a series of 5% (*x*Ni*y*Co)/SBA-15 catalysts synthesized via a modified co-impregnation method. They found that the alloying of Ni and Co was the key factor for improving the catalytic

performances, owing to the increase in CO_2 dissociation and the metal reducibility, however the Co:Ni ratio was an important factor impacting the success of the catalyst. They concluded that the addition of trace amounts of Co enriched on Ni-Co surface prevented the sintering of metal particles and facilitated the adsorption of CO_2, thus improving the overall catalytic stability. TGA curve results of spent catalysts suggested that after doping Co, the carbon deposition and self-carbon elimination was approximately balanced on the 4.5Ni0.5Co/SBA-15-CD [123].

A higher Co content was also reported to improve catalytic performance during TOS by San-José-Alonso et al. They found that the optimum activity and stability were achieved with catalysts containing high Co loadings. Among the catalysts studied, the samples with the highest cobalt content displayed the highest activity and stability, but also a large amount of carbon deposition. They attributed the higher activity and stability observed on the Co-rich catalysts to the higher activity of Co for methane decomposition and to the presence of large particles involved in long-term conversion, producing non-deactivating carbon deposits [17]. Horlyck et al. evaluated Ni-Co/Al_2O_3 synthesized via impregnation with various Ni-Co content. They reported that the coupling of Ni and Co allowed for both the activity of Ni and the resistance of Co to deactivation (via carbon formation) to be captured, with the extent governed by the ratio of the two metals. NiCo(7.5-2.5) displays the highest methane conversion, followed by NiCo(5-5) and NiCo(2.5-7.5). NiCo(5-5) was found to have the highest CO_2 conversion. However, detailed characterization of spent catalysts revealed that NiCo(7.5-2.5) had higher carbon content resulting from methane decomposition, and NiCo(2.5-7.5) higher carbon content resulting from Boudouard reaction, as shown in Table 5. They concluded that (i) the high CH_4 conversion exhibited by NiCo(7.5-2.5), NiCo(5-5) and NiCo(2.5-7.5) during the DRM arose from Ni content leading to an increased affinity for CH_4 activation; (ii) carbon formed on the Co and NiCo from the Boudouard reaction is active and readily oxidized to CO, whereas the carbon species on Ni are less readily oxidized and lead to deactivation during the DRM reaction, as shown in Fig. 10 [124].

Table 5. TGA Analysis of spent catalysts showing BET specific surface area and total carbon content after performance testing of bimetallic NiCo catalysts for the DRM reaction. Reproduced from Ref. [124].

Sample[#]	BET specific surface Area (m^2/g)	Carbon content after testing (wt%)			
		DRM light-off	DRM Stability	Boudouard	CH_4 Cracking
Ni(10)	143	14.0	39.5	25	41.3
NiCo(7.5-2.5)	129	1.7	4.1	9.6	22.5
NiCo(5-5)	134	2.5	21.2	25.6	6
NiCo(2.5-7.5)	133	2.1	3.7	51.6	2.8
Co(10)	117	1.3	0.0	48.5	3.1
Al_2O_3	142				

[#] Values in brackets represent nominal Ni/Co loadings on the catalysts (wt%).

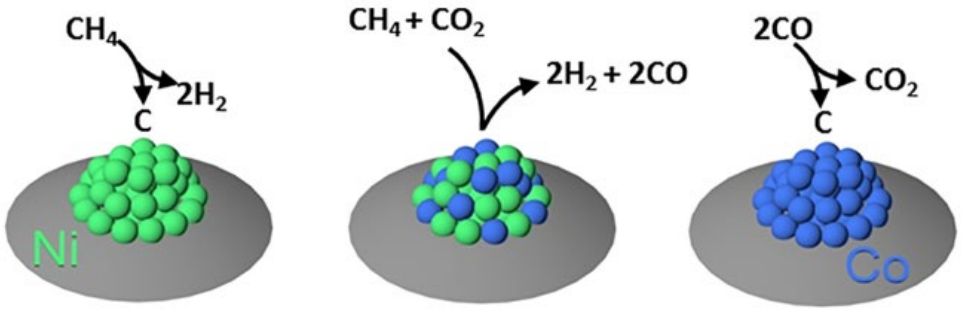

Fig 10. Illustration of active metals (Ni and Co) in Ni-Co bimetallic catalysts towards the Boudouard, methane cracking and reverse water gas shift side reactions. Reproduced from Ref. [124].

San-José-Alonso et al. reported that Co-rich Ni catalysts showed enhanced activity for methane decomposition, which has been considered as the rate determining step of the DRM reaction [27]. This is because the formation of the bimetallic alloy also modifies the oxophilicity and results in different surface intermediates for the DRM reaction. Commonly, transition metals display a tendency towards the formation of oxides by hydrolysis or abstraction of an oxygen atom from another molecule. Through both kinetic data and in-situ X-ray absorption spectroscopy (XAS) obtained for monometallic Co and Ni, as well as bimetallic Ni-Co, Al Sabban et al. found that the Ni catalyst experienced carbon deposition, while the bimetallic CoNi catalyst, at all mass ratios evaluated, showed a negligible amount of deposited carbon, likely the result of balancing the oxidative (CO_2 and H_2O) and reductive (CH, CO, H) species on the catalyst surface. In comparing the monometallic Co and Ni and bimetallic CoNi catalysts, they found direct experimental evidence for the oxidation of Co under DRM conditions, while CoNi and Ni maintained their reductive form. Due to the low coverage of the oxygen species on the surface of the monometallic Ni catalyst, a diminished removal of the carbonaceous deposits formed from the CO disproportiation was observed, resulting in an accumulation of carbon on the surface. DFT calculations confirmed that alloying Ni and Co enabled control over the oxophilicity of the catalyst in order to balance the kinetics of DRM [120]. Wu et al. also found that the high performance of the Ni-Co bimetallic to be attributed to the formation of the alloy under reaction conditions, which favors the CO_2 dissociation and increases the metal reducibility when evaluating Ni_xCo_y nanocatalysts [123]. Sheng et al. noted that the coexistence of Ni and Co helps to balance the number of carbon species derived from CH_4 decomposition and oxygen species from the reduction of CO_2, which effectively avoids coke accumulation and catalyst oxidation. They proposed a synergistic mechanism to explain the kinetics of the DRM reaction, where Ni and Co were catalysts for CH_4 cracking and CO_2 reduction, and the induced carbon deposits and active oxygen combined to release CO, thus regenerating the metal surface for the next-round reaction [125].

Tu et al. conducted both experimental studies and DFT calculations to explore the distinct for C-H bond activation for DRM over Ni, Co, and Ni-Co clusters and identified the role of the reactive oxygen species on metal active sites. They found that the presence of reactive oxygen species promoted the removal of carbonaceous intermediates (CH_x^*) during DRM resulting in high availability of the active sites for C–H bond activation [126]. As previously noted, CH_4 decomposes only on the metal surface, whereas CO_2 can also be activated on the support [6]. Zhang et al. studied both monometallic Ni/TiO_2 and Co/TiO_2, as well as bimetallic $Co–Ni/TiO_2$ for DMR. Using CH_4 pulse reaction, they reported a decrease of CH_4 decomposition activity for the bimetallic catalyst as a result of the oxygen affinity of Co, attributed to suppression of metal

oxidation during the DRM reaction. Because higher activity for CH_4 decomposition results in a greater number of coke species on the surface of the metal, which ultimately becomes deactivating carbon, the bimetallic control of CH_4 decomposition activity results in a higher tolerance to carbon formation than that of the monometallic Ni catalyst [114]. The results of Wu and coworkers also noted that exposed active Ni metal surface was the active site for the activation of CH_4, though Co was also considered to be active site for CH_4 decomposition [115]. Furthermore, adjusting the composition of Ni and Co enabled kinetic control over the elementary steps of the DRM reaction, namely the formation of carbon species and their removal by oxygen species. Consequently, the formation of Co and Ni bimetallic catalysts inhibited both the oxidation of Co and the carbon deposition over Ni [121].

Overall, Ni-Co bimetallic catalysts are very promising for the DRM reaction due to the coupling of the high activity of Ni with the high resistance of Co towards carbon deposition, resulting in an active, selective, and stable catalyst for the DRM reaction. The promotional effect of Co is mainly attributed to its strong affinity for oxygen species that enhances the adsorption of CO_2, thus helping the inhibition of carbon deposition by enhancing carbon removal. In addition, the synergism between Ni and Co assists in the dispersion of the active sites of the metal alloy leading to an improved overall catalytic performance.

3.2 Other Ni-based bimetallic catalysts

The Ni-based catalysts have shown promising results for DMR, with Ni-Co materials being the most extensively investigated bimetallic catalysts. Additional studies have been performed to compare the modification of Ni by other elements, including both non-precious and precious metals. As summarized below, these bimetallic catalysts have also been reported to be beneficial to increasing the overall coke resistance of the catalysts [127].

3.2.1 Ni promoted with non-precious metals

The durability of Ni-based catalysts can be enhanced by the addition of another metal, forming a bimetallic alloyed structure. The formation of these bimetallic alloys has shown promising results both in terms of high activity and stability. Liu et al. evaluated a series of confined indium-nickel (In-Ni) intermetallic alloy nanocatalysts and found that $InNi@SiO_2$ alloy showed superior coking resistance in the DRM reaction, attributed to the synergy of In and Ni. The increased carbon resistance was accredited to the confinement of the core–shell structure, coupled with the transfer of electrons from In to Ni in the In-Ni intermetallic alloys due to the smaller electronegativity of In [128]. Wan et al. evaluated various Ni–Fe/Mg(Al)O alloy catalysts and reported that the formation of the Ni-Fe alloy contributed to the uniform composition and size-controllable bimetallic particles. Characterization of spent catalysts revealed that the reduced catalysts showed higher coke resistance as a result of the small particle size [129]. Yusuf et al. compared the performance of Ni monometallic Ni-W bimetallic catalysts for the DRM reaction. Based on the results of their study, they reported that W and Ni appeared to form an alloy that proved beneficial to the performance of the catalyst during time-on-stream (TOS). The alloy was uniformly dispersed onto an Al_2O_3-MgO support. The temperature-programmed reduction (TPR) results confirmed that addition of W enriched degree of reduction, creating more nickel active sites to be used during the reaction. Furthermore, elemental mapping results verified the enhanced metallic distribution for the bimetallic Ni-W as compared to that of the monometallic Ni, because the alloy formed did not allow the Ni to agglomerate. From H_2-TPR results, the authors reported that the

Ni-W catalyst showed enhanced Ni dispersion after W addition, as reflected by higher H_2 consumption. This led to a greater number of active sites available for the DRM reaction, and thus increased the amount of carbon deposition required to deactivate the catalyst [130]. Guharoy et al. reported that Ni-Sn bimetallic catalysts showed minimal deactivating effects resulting from carbon deposition. The durability of the Ni-Sn bimetallic alloy was attribute to its increased dispersion of the metallic particles on the catalyst [131].

The effect of catalyst particle size on thermodynamic equilibrium of methane dry reforming and carbon deposition has been extensively reviewed and it has been found that carbon formation decreases with a decrease in particle diameter. Sintering of the Ni particles during operation leads to a loss of dispersion, ultimately leading to catalyst deactivation and increased carbon formation; carbon layers that grow from nuclei on step sites on the Ni particle are stable above 80 atoms in diameter (approximately 6 nm), meaning that larger particles are more likely to yield carbon [132]. Song et al. evaluated a Mo-Ni bimetallic catalyst and found that the small bimetallic particles led to reduced coke formation and increased resistance to sintering and catalyst deactivation [133]. Similarly, Dehimi et al. observed a synergistic interaction between Mo and Ni, reporting that smaller particles and alloy formation led to minimal coke formation. Temperature programmed reduction studies indicated the presence of amorphous carbon [134], which was more reactive than filamentous or graphitic carbon [135]. An increase in Ni percentage in the catalyst formulation from 20Mo2Ni to 20Mo10Ni supported on alumina enhanced the dispersion of Mo species, corresponding to an increased catalytic activity. As evidenced by H_2-TPR profiles, no graphitic carbon peak was observed for the 20Mo10Ni when compared with 20Mo2Ni [134]. Similarly, Huang et al evaluated an Mo-Ni catalyst synthesized on SBA-15 and reported the same beneficial effect of small metal particle size with increased metal dispersion over the support, resulting in the prevention of carbon formation around the catalyst particles [136]. Shamskar et al. evaluated La-, Ce-, and Zr- promoted Ni-Al_2O_3 catalysts. Fig. 11 displays the H_2-TPR analysis of the 25Ni-CeO_2-Al_2O_3 catalysts with different Ce loadings. All catalysts showed two main reduction peaks at 600–800 °C. The first peak located around 650 °C is attributed to the NiO species strongly interacted with the spinel. The other peak located at around 800 °C is assigned to the $NiAl_2O_4$ phase. The low temperature reduction peak (300–400 °C) related to NiO species was not observed, confirming the absence of bulk NiO particles [137]. Momteiro et al. investigated the reducibility of CeO_2 supported on Al_2O_3 [138]. They showed that the reducibility of Ce was related to the content of ceria and the reduction was incomplete in samples with low content of CeO_2 (3% CeO_2). Yang et al. proposed that the amount of carbon deposition was significantly reduced due to alkaline function and dispersion enhancement of CeO_2, as well as the electronic interactions between CeO_2 and Ni. Characterization of the spent catalyst using SEM revealed the presence of a moss-like carbon on the 10%Ni/γ-Al_2O_3 catalyst that was not easily gasified with CO_2.Conversely, the presence of filamentous carbon on the CeO_2 and La_2O_3 promoted Ni-based catalysts was able to be easily eliminated. They attributed the stable catalyst activity of the promoted Ni catalysts to the suppression of Ni particle sintering and the formation of the reactive filamentous carbon [139]. Similarly, Chein and Fung agreed with these findings, showing that a 5 wt% CeO_2 catalyst enhanced the dispersion of Ni particles [140]. In addition to improving the dispersion of nickel, ceria is also believed to increase surface area and decrease the nickel particle size [141]. Liu et al. evaluated MCM-41 supported Ni-based bimetallic catalysts promoted with Zr, Ti, and Mn. They reported that all Zr-promoted catalysts exhibited comparable or enhanced initial catalytic activity as compared to Ni–MCM-41, noting that the addition of Zr^{4+} improved the long-term stability, as

compared to Ti- and Mn- modified catalysts, which were found to have a lower initial activity and stability. Further characterization of the catalysts revealed that the addition of Zr^{4+} enhanced the structural stability and the dispersion of the active Ni sites. Their finding revealed that Zr addition to the Ni-based catalysts decreased overall particle sizes [142]. Lu et al. evaluated a series of vanadium-doped Ni_x-V-MgAl catalysts for the DRM reaction. They found that the addition of V to a Ni-based catalyst enhanced CO_2 activation ability of the Ni_{10}-V-MgAl catalyst and curtailed the generation of carbonaceous deposits, leading to an enhanced stability in long-term testing compared to undoped Ni-MgAl [143].

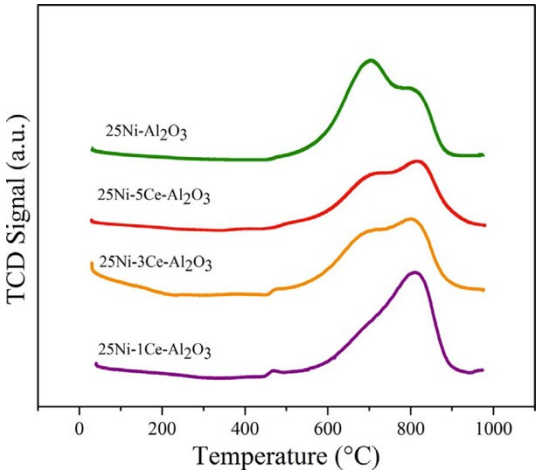

Fig. 11. H_2–TPR profiles of the 25Ni-CeO_2-Al_2O_3 catalyst with different Ce loadings. Reproduced from Ref. [138].

Wan et al. found that, due to the synergistic interactions of Ni-Fe, the bimetallic catalysts inhibited the dissociation of methane as a result of the ensemble effect, which was believed to play a major role in the suppression of coke deposition. Furthermore, the addition of Fe to Ni-catalysts promoted CO_2 activation at the metal-support interface as well as the Fe sites to provide adsorbed oxygen, which reacted with carbon to recover the active surface. The inhibition of CH_4 dissociation, coupled with the activation of CO_2, helped to establish a dynamic balance between carbon generation and removal, leading to less coking [129]. Theofanidis et al. evaluated the redox properties of Ni-Fe bimetallics using a series of Fe-Ni/$MgAl_2O_4$ catalysts with various Ni:Fe loading for DRM. The elemental distribution of 0.7-Fe/Ni is illustrated in Fig. 12 (a-b) using energy-dispersive X-ray spectroscopy (EDX)-STEM mapping. Both Fe (red) and Ni (green) were distributed uniformly in the sample after reduction, implying the alloy formation. In contrast, after CO_2 oxidation the Ni and Fe particles were segregated as Fe was oxidized to Fe_3O_4 and the Fe-Ni alloy was decomposed to metallic Ni, as illustrated in Fig. 12c. Metallic Ni remained stable under a CO_2 flow and was not oxidized to NiO [144]. Though Ni-Fe alloy is the active phase, Fe partially segregates from the alloy during DRM forming FeO species, which reduces surface carbon accumulation through an interaction with the lattice oxygen of the FeO, which leads to the production of CO. Furthermore, Yentekakis et al. reported that the presence and migration of FeO at the catalyst surface enables it to react with deposited carbon. The rapid removal of Ni-C species by Fe due to its alteration of the carbon gasification mechanism, improves coke tolerance through the addition of the Ni-Fe alloy particles, which could further recover to their original structure after carbon removal by re-alloying during catalyst reduction, as shown in Fig. 13 [145].

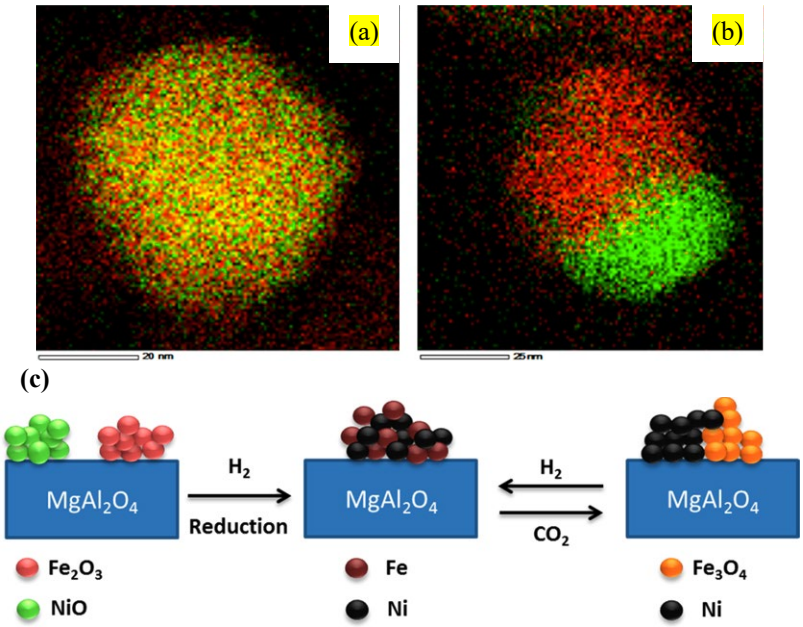

Fig. 12. EDX element mapping of 0.7-Fe/Ni: (a) after H_2 reduction; (b) after CO_2 oxidation. Red and green colors correspond to Fe and Ni elements, respectively). (c) Schematic diagram of Fe-Ni alloy formation, during H_2-reduction, and decomposition, during CO_2 oxidation. Reproduced from Ref. [144].

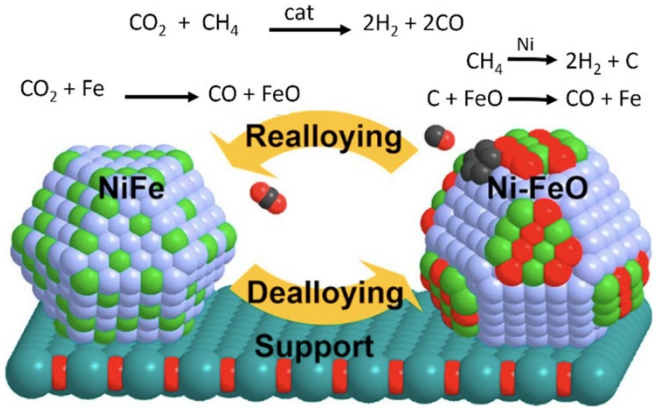

Fig 13. Redox mechanism of FeO in restoring NiFe alloy and removing carbon deposits. Reproduced from Ref. [145].

Guharoy et al. reported that Sn-Ni bimetallic catalysts increased carbon resistance through an increase in the activation energy barrier of atomic carbon formation on the catalyst surface. Methane dissociation rates decreased with increasing concentrations of Sn, although too high of a concentration was believed to hinder activity by reducing the number of active sites. Carbon deposited on the bimetallic catalyst surface was less graphitized and less harmful to the active sites compared to that on monometallic Ni, resulting in an enhanced stability of the catalyst and reduced deactivation rates [131]. The effect of Cu on carbon formation on Ni catalysts was also found by Qiu et al. and Omran et al., who reported that the addition of Cu made CH able to be more easily oxidized rather than dissociated. Cu was found to reduce coke deposition by increasing of the activation energy barrier of CO* and CH* dissociation. Further, the removal of carbon, via O* +

C* → CO*, was enhanced in the Cu-Ni bimetallic system compared to the monometallic Ni catalyst [146,147].

It has also been found that the formation of an oxide species can increase the interaction of Ni with oxygen, increasing the overall stability of the catalyst and its resistance to deactivation. Ni–Mo bimetallic catalysts with strong metal–support interaction effectively prevented the formation of shell-like carbon deposit [136], which was attributed to the property of CO_2 adsorption and activation [148]. The carbon species formed on the support and on the metal were removed by reaction with adsorbed oxygen species. Furthermore, it was found that the formation of Mo_2C in bimetallic catalysts prevented the growth of Ni particles effectively. The Ni–Mo bimetallic catalysts not only have good resistivity to coking and sintering but also change the kinds of carbon deposits; consequently, the bimetallic catalysts have high activity and excellent stability [136].

Some forms of coke deposition result in loss of catalytic activity, while others do not. This is dependent on the reactivity of the carbon species, as well as the structure of the carbon species formed. Yusuf et al. found that in Ni-W bimetallic catalysts a tungsten-carbide formed that was thought to activate CO_2 into carbon monoxide and O*. The formation of this carbide was reported to hinder the formation of coke. Furthermore, on the Ni-W bimetallic, they reported the formation of multi-walled carbon nanotubes (MWCNT), as compared to the formation of amorphous carbon nanosheets that encapsulated a metal particle on the monometallic Ni catalysts, as shown in Fig. 14 [130]. MWCNTs are less deactivating to the catalyst due to their tube-like structure piled one on top of another.

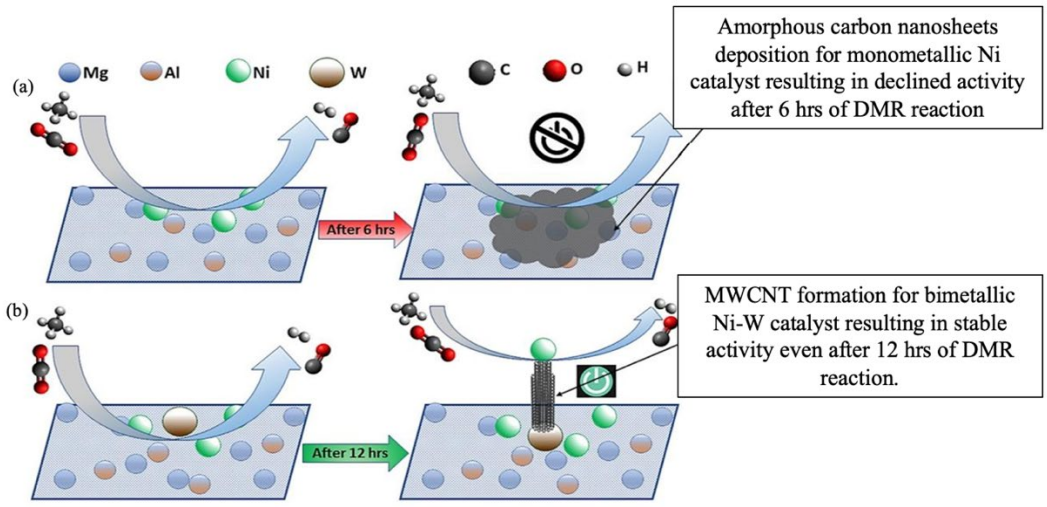

Fig 14. Effect of W-promotion in Ni-based catalysts. (a) Ni/Al_2O_3-MgO catalyst deactivates due to formation of amorphous carbon nanosheets. (b) $Ni-W/Al_2O_3$-MgO catalyst remained active due to formation of MWCNT. Reproduced from Ref. [130].

Huang et al. reported a similar synergistic effect between Mo and Ni, where $CO_2$was able to adsorb and dissociate on the catalyst surface more efficiently than in the monometallic counterpart. The increased ability of the Ni-Mo catalysts to eliminate the intermediate carbon species formed by methane decomposition was attributed to its contribution of enough oxygen species for the gasification of undesired carbon intermediates. Characterization of spent Ni-Mo catalysts via TEM

found that, on the catalyst, all carbon deposition formed whisker-like carbon nanotubes that were not deactivating to the bimetallic catalysts in the DRM reaction [136]. Aramouni et al. also reported the formation of a whisker-like carbon on a similar Mo-Ni bimetallic catalyst on Al_2O_3 support [70]. This type of non-deactivating carbon deposition was thought to be attributed to the presence of metallic Mo.

3.2.2 Ni Promoted with precious metals

Precious metals such as Pt, Rh or Ru display reduced sintering, high resistance to coke deposition and high catalytic activity. However, practical use of monometallic precious metal catalysts is hindered due to high cost and limited availability. These catalysts perform better because they can disperse on their support and retain small particle size. Furthermore, they tend to reduce the amount of coke formed during the DRM reaction [15]. Therefore, in order to leverage the advantageous properties associated with precious metals, bimetallic catalysts have been explored for their ability to mitigate catalyst deactivation due to the synergistic effect of the two active metals.

Doping Ni with small amounts of precious metals not only enhances the DRM, but it also minimizes catalyst deactivation resulting from carbon deposition. While studying the use of Pd on bimetallic Ni-based catalysts supported on mesoporous silica for activity in DRM, Pan et al. discovered that adding traces of Pd to Ni aided in suppressing buildup of graphitic carbon on the catalyst surface [149]. Steinhauer et al. noticed the same trend while studying the effect of varying catalyst supports for bimetallic Ni-Pd. Characterization by X-ray photoelectron spectroscopy (XPS) demonstrated that the interactions between Ni and Pd allowed for the reduction and distribution of nickel particles [150].

Pt is another precious metal known to be highly active and resistant to carbon deposition for the DRM reaction, but it is not widely utilized due to its high cost. Araiza et al. observed that as the amount of Pt loading increased, the amount of carbon deposition decreased due to the enhanced synergistic properties of Pt and the ceria support, which helped to remove carbon deposits. However, the authors also discovered that among their monometallic and bimetallic catalysts, $Pt_{25}Ni_{75}$/Ce produced the highest amount of carbon deposition, despite not having the lowest level of stability. On the other hand, the monometallic Pt/Ce catalyst produced the least amount of carbon deposits yet had higher rates of deactivation compared to the bimetallic catalyst, thus indicating that deactivation of Pt-containing catalysts is not highly dependent on carbon deposition [151]. Likewise, Li et al. reported in their findings that bimetallic NiPt(0.71)/Al_2O_3 had the lowest rate of carbon formation in comparison to the other metal loading ratios containing smaller amounts of Pt. When comparing their monometallic Ni and Pt catalysts, the group observed that the Pt/Al_2O_3 catalyst deactivated due to sintering while the Ni/Al_2O_3 catalyst deactivated due to the formation of carbon. After performing DFT calculations, the authors attributed the superior performance of the Ni-Pt bimetallic to enhanced catalytic activity and suppressed carbon formation as the Pt coverage increased [152]. Meshkani and Rezaei attributed the high stability of their bimetallic Ni-Pt/MgO catalyst to the ability of Pt to increase nickel dispersion. Higher Pt loading on the catalyst led to more highly dispersed Ni particles, which contributed to a decrease in coke formation, as reflected by the temperature-programmed oxidation (TPO) profiles. Furthermore, the results of thermogravimetric analysis (TGA) showed that the carbon formation over the bimetallic catalyst was much lower than that of monometallic 5% Ni/MgO [153]. In addition to enhancing Ni dispersion, Pt was also capable of reducing the activation energy of methane and

CO_2 by the catalyst, leading to an enhanced surface oxygen reactivity. This occurrence resulted in an increase in coke resistance due to the enhanced O* reactivity that promoted higher levels of activity and surface carbon cleaning [152].

Tsyganok et al. investigated several $MgAlO_x$-supported Ru-based bimetallic catalysts synthesized using repeated "calcination-reconstruction" cycles and LDH structured catalyst precursors. Compared to the other Ru-based bimetallic catalysts, the combination of Ni and Ru demonstrated notable synergistic interactions. The Ru-Ni catalyst was shown to reduce the rate of coke formation during pre-calcination of its LDH precursor, a finding similar to that of when an in situ–formed Ru-Ni catalyst was obtained. In contrast, the amount of coke formation for a pre-calcined monometallic Ni catalyst was found to be over twice the amount of coke deposited on the in situ-formed catalyst [154]. Mahfouz et al. explored monometallic and bimetallic catalysts containing Ru and Ni supported on mesoporous KIT-6. The benefits of doping Ni with Ru were evident when comparing the amount of carbon deposition between monometallic Ni/KIT-6 and bimetallic Ni-Ru/KIT-6 using differential thermal analysis (DTA) curves to quantify weight loss of the catalysts, which were 40% and 5%, respectively. The decreased weight loss of the bimetallic was said to be due to the ability of Ru species to provide a reactional pathway to adsorbed carbon species, thus transforming them into gaseous compounds. By incorporating Ru within close proximity to the active sites of Ni, the reduced surface is stabilized, limiting the accumulation of carbon inside the nickel particles by promoting carbon gasification. This was likely due to the activation of water molecules formed during the RWGS reaction, which were then able to react with the adsorbed carbon species on the catalyst [155]. The addition of Ru not only hindered the accumulation of carbon on the Ni particle but also facilitated the formation of a reactional pathway for the removal of adsorbed carbon species, transforming them into gaseous compounds. The authors noted that the process of continuous carbon gasification may even allow for the regeneration of active sites. Crisafulli et al. compared bimetallic Ni-Ru catalysts supported on silica and H-ZSM5 zeolite in terms of activity and stability in DRM. The results indicated that bimetallic Ni-Ru catalysts performed better on silica than H-ZSM5 zeolite in both activity and stability. High enhanced stability in the bimetallic catalyst supported on silica was due to the formation of Ni-Ru clusters, leading to an increase in Ni dispersion. Larger loading of Ru in Ni-Ru/SiO_2 samples was found to be responsible for enhancing H_2 and O_2 uptake indicating that Ru was the main contributor to high Ni dispersion, and thus responsible for lower levels of carbon formation [156]. In another study comparing the effects of varying supports, Andraos et al. investigated DRM performance using monometallic and bimetallic Ni-Ru catalysts supported on Al_2O_3, $MgAl_2O_4$, and YSZ. They found that bimetallic Ni-Ru catalysts had higher resistance to coke formation when supported by Al_2O_3 and $MgAl_2O_4$, attributed to the presence of Ru [157]. However, a reduced DMR activity was observed in Ru-containing catalysts. Similarly, Álvarez M. et al. noticed that the monometallic Ru catalyst was the least active in DRM. Regardless, catalysts containing Ru exhibited high stability and low carbon formation. Ru was also noted to prevent the formation of nickel carbide, which was suggested to be the main precursor to carbon deposition [158].

Mozammel et al. found that doping Ni with Rh improved methane and CO_2 conversion. Furthermore, they reported that the bimetallic Ni-Rh catalyst supported on mesoporous alumina exhibited high levels of activity and stability for DRM. The high resistance to coke formation over the bimetallic catalyst was attributed to the addition of Rh, which was capable of enhancing carbon gasification reactions by the hydrogen spillover effect, as well as oxidation of carbon by CO_2 [159].

3.3 Other bimetallic catalysts

In addition to Ni-based catalysts, Co-based bimetallic catalysts have also been extensively investigated for DRM. The relative abundance Co makes it a viable option for industrial use. Introducing a second metal to Co to form a bimetallic catalyst could not only improve DRM activity, but also decrease carbon deposition and mitigate catalyst deactivation. Özkara-Aydinoğlu and Aksoylu investigated the performance of Co-based catalysts supported on ZrO_2 for DRM, using various metal promoters (La, Ce, Mn, Mg, K). Results showed that monometallic Co outperformed most of the bimetallic catalysts in initial methane conversion. However, the activity was quickly reduced due to the formation of filamentous carbon, as shown in Fig. 15. Among the various catalysts, Co-K and Co-Mg deactivated the most rapidly due to coke formation. The authors attributed the rapid deactivation to large particle size and low metal dispersion induced by the formation of Co clusters. Mn was found to enhance metal dispersion, slowing the process of coke formation. La-promoted Co catalysts showed the most stable performance, though only moderate activity, as well as no detectable carbon deposition due to highly dispersed small metal particles. However, the authors discovered that the addition of a small amount of Ce to Co resulted in the best overall performance and resistance to carbon deposition. This was attributed to the increased amount of cobalt covering the surface of the catalyst, as well as the enhanced ability to gasify coke. Because of the high oxygen storage capacity cerium oxides, especially when combined with ZrO_2, the $Co/CeO_2/ZrO_2$ catalysts facilitated the production of mobile surface oxygen and the enhancement of oxygen transfer, enabling Co to become more resistant to carbon deposition [160]. In a separate study, Paksoy et al. studied the DMR performance of $Co\text{-}Ce/ZrO_2$ catalysts. The continuous redox cycle that the Ce center enhanced oxygen transfer to Co centers, thus resulting in the removal of deposited carbon through oxidation, causing the catalytic centers to become more resistant to the formation of carbon. Thus, less carbon is observed to form on regions of high Ce/Co ratio, as indicated by the circles in Fig. 16 [161].

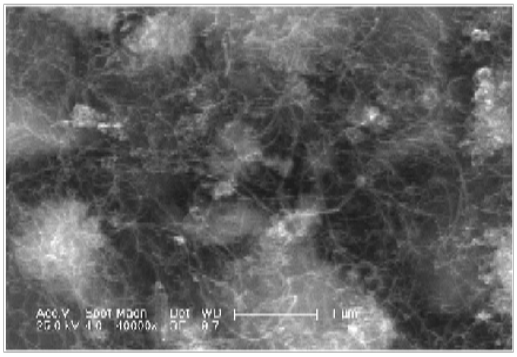

Fig 15. Field emission scanning electron microscopy (ESEM) characterization of carbon deposition morphology on unpromoted 5Co sample after 6 h of DRM reaction depicting filamentous-type carbon over catalyst surfaces Reproduced from Ref. [160].

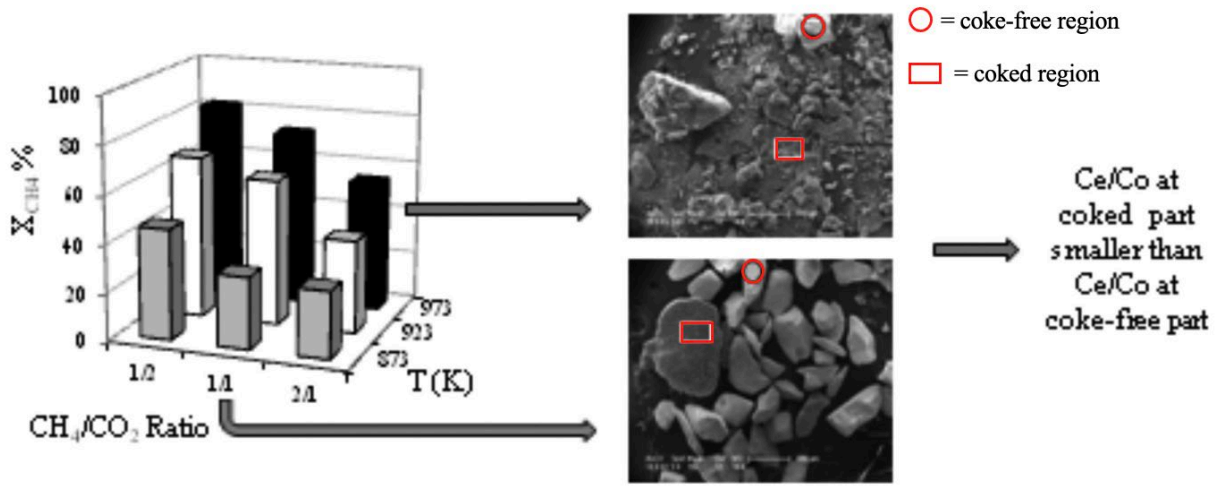

Fig 16. Characterization of Co-Ce catalysts (a) time-on-stream activity and selectivity profiles terms of CH_4 conversion % under different CH_4/CO_2 feed ratios and temperatures; (b) SEM images at 973 K and CH_4/CO_2 = 1/1, showing Ce/Co molar ratio was greater at coke-free parts and confirming that the presence of ceria on the surface increases CO_2 dissociation and generating surface oxygen. Reproduced from Ref. [161].

Pang et al. investigated nanostructured bimetallic Ru-Co@SiO_2 catalysts for DRM. XRD patterns of the spent catalysts demonstrated that at higher temperatures, Ru-Co@SiO_2-P did not form carbon species on its surface. The addition of Ru to Co was found to potentially inhibit oxidation of Co. Furthermore, the even distribution of Ru over Co allowed for weaker adhesion of surface carbon, thus reducing the amount of carbon deposition [162]. According to Aramouni et al., Ru was also capable of enhancing the dispersion of Co, which allowed the bimetallic 15Co-0.25Ru catalyst to remain stable and active despite the high levels of coking [79]. In a separate study, Tsyganok et al. examined Ru-based bimetallic catalysts supported on Mg-Al mixed oxides. The authors investigated the synergistic effects of Ru with five transition metals (Cr, Fe, Co, Ni, and Cu). TG-DTA results (Fig. 17) showed that among the five bimetallic catalysts, Ru-Cu formed the least amount of coke, 9.8 wt%, while the other catalysts formed approximately 30 wt% of coke [154].

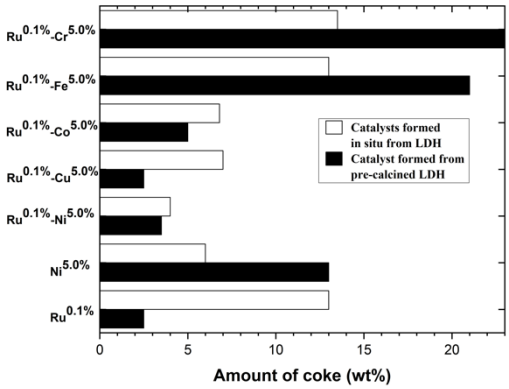

Fig 17. TPO estimation of coking capacity over bimetallic catalysts after the DRM reaction at 800 °C for 6 h measured by temperature-programmed oxidation: air flow, 40 cm^3 min^{-1}; pressure, 1 atm; heating rate, 2.5 °C min^{-1}. Reproduced from Ref. [154].

El Hassan et al. explored how doping Co/SBA-15 catalysts with small amounts of Rh may affect coking during the DRM reaction. Fig. 18 displays the distribution of the different coke species deposited on the monometallic and bimetallic catalysts. The authors reported a direct correlation in the formation of C_α as a result of the active metal loading: an increase in the loading of Rh resulted in an increase in the amount of atomic carbon. However, C_α was formed as a reaction intermediate and did not contribute to deactivation. Results showed that higher amounts of formation of graphitic carbon, C_γ, were found on monometallic catalysts, forming almost four times more than the bimetallic catalysts. $Rh_{0.5}Co_{12}$/SBA-15 exhibited the lowest amount of graphitic C_γ and was thus the catalyst that was least prone to deactivation, despite forming the most C_α [163]. These findings revealed the positive synergistic effects of Co and Rh in reducing the detrimental effects of carbon deposition.

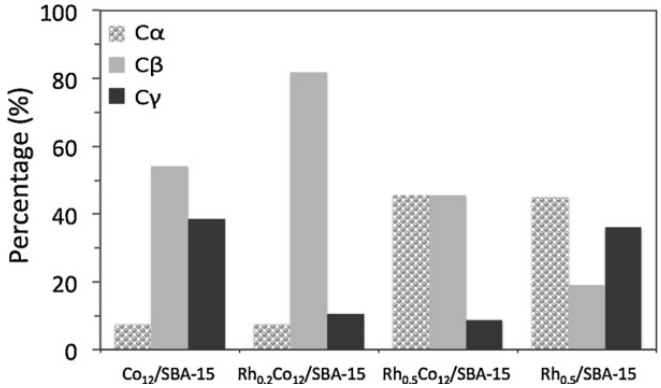

Fig 18. Percentages of different types of coke C_α, C_β and C_γ on the spent catalysts deduced from combined temperature programmed hydrogenation and mass spectrometry profiles for Co_{12}/SBA-15, $Rh_{0.2}Co_{12}$/SBA-15, $Rh_{0.5}Co_{12}$/SBA-15 and $Rh_{0.5}$/SBA-15 catalysts. Reproduced from Ref. [163].

In a study comparing DRM performance of monometallic Pt and Co with that of bimetallic Pt-Co catalysts supported on CeO_2, Xie et al. established that the bimetallic catalyst showed the highest activity. However, the opposite trend was true in terms of catalyst stability. Pt-Co produced the highest amount of carbon deposition, while the monometallic catalysts generated trace amounts. Low levels of carbon deposition in the Co monometallic catalyst were due to the low activity of Co/CeO_2 whereas the coke resistant properties of the monometallic Pt catalyst were attributed to the O* modified surface of Pt/CeO_2. Although the $Pt\text{-}Co/CeO_2$ catalyst displayed a considerable amount of coke formation, when accounting for catalyst activity levels, the bimetallic catalyst was found to be relatively as effective as monometallic Pt at resisting coke formation. [164]. Similarly, while evaluating Pt-Co and Ru-Co supported on TiO_2, Nagaoka et al. found that adding trace amounts of Pt to Co significantly improved resistance to coking. Although the addition of Ru and Pt both improved the DRM performance, Pt was able to effectively induce similar levels of activity and stability as Ru, with less than half the amount of precious metal loading [165].

Though not as favored as Ni or Co, Mo is another transition metal that has been extensively explored for use in DRM. Jawad et al. compared monometallic Mo, bimetallic Pt-Mo and Fe-Mo, and trimetallic Pt-Fe-Mo catalysts for DRM activity. The bimetallic Pt-Mo catalyst formed less carbonaceous deposits, as compared to the monometallic catalysts and other bimetallic catalysts. The presence of precious-metal Pt increased the basicity of the catalyst, thus enhancing the rate of activation of CO_2. This resulted in promoted oxidation of surface carbon and a decreased rate of deposition. In addition, catalysts doped with Mo were reported to have a sufficient amounts of

oxygen species necessary to gasify carbon intermediates as a result of improved CO_2 chemisorption and dissociation. When small amounts of Mo were added to Ni, the bimetallic catalyst improved in stability and formed higher levels of CO, preventing the accumulation of carbonaceous deposits. Furthermore, the authors reported the formation of molybdenum carbides when the catalyst was doped with Mo, which also contributed to a higher resistance to coking [166]. When Mo was added to Co-based catalysts, both Fu et al. and Nguyen et al. reported the synergistic effect between the two transition metals, resulting in a higher resistance to coke formation [167,168]. In the case of the Co-Mo/TiO_2 catalyst, a significantly low level of coking was attributed to the enhanced rate of oxidation of the deposited carbon [167]. The authors hypothesized that the surface carbon was removed as a result of gasification reactions involving H_2O and CO_2. Nguyen et al. also investigated bimetallic Co-Mo catalysts supported on Al_2O_3 with varying metal loadings, with. a Co/Mo ratio of 2 being the best resistance to carbon deposition [168].

4. Conclusions

Due to the highly endothermic nature of the DRM reaction, the required reaction temperatures result in rapid carbon deposition and catalyst deactivation, although the CO_2/CH_4 reactant ratio, reaction pressure, and reaction temperature all have a considerable influence on the equilibrium of the reactant conversions and solid carbon formation [75]. Many attempts have been made to control coke deposition, or minimize its impact, at a catalyst level such as alterations in the morphology of the metal (changing particle size) [75], changing the chemical environment of the metal [103], utilizing a different synthetic pathway [108], or incorporating another metal into the catalyst to form bimetallic catalysts [145].

The use of bimetallic catalysts has proven to enhance the activity and stability of the catalyst due to the synergistic interactions between the two active metals. Currently, bimetallic catalysts for DRM have generally focused on combinations of Ni with a precious metal (such as Pt, Rh, Pd) or Ni coupled with another earth abundant transition metal. The benefits of bimetallic catalysts over their monometallic counterparts have been attributed to the structural and electronic modifications resulting from the formation of the bimetallic bonds, leading to an enhanced DRM performance.

The results summarized in this review have suggested that the incorporation of a precious metal into a Ni-based catalyst results in improved reducibility and resistance to oxidation, agglomeration, and coking. This has been attributed to the dilution effect of precious metals, thus leading to smaller metal particles with a higher overall dispersion and preventing agglomeration of metallic particles and catalyst deactivation. Bimetallic combinations of earth abundant transition metals, such as Ni-Co, Ni-Fe, Co-Mo, have also shown great promise towards reducing coke formation on the catalysts during DRM. Among the various bimetallic catalysts, Ni-Co alloys have been comprehensively investigated in DRM for their improvement on metal dispersion and their ability to abate carbon deposits on the surface of the catalysts, attributed to the high oxygen affinity of Co favoring carbon removal. Similarly, Ni-Fe bimetallic catalysts have been found to promote carbon removal, and thus the performance of the catalyst. The incorporation of Co into Mo-based catalysts has shown to improve carbon gasification. Furthermore, the tuning of the metallic ratios utilized in the bimetallic catalysts has been found to profoundly affect the performance of the catalysts. For example, it has been shown that a small Co amount may benefit carbon removal of Ni-based

DMR catalysts; however, a large amount of Co may result in a reduction in DRM activity due to enhancement in particle oxidation [145].

While the quantity of coke content is generally used as a measure for the extent of catalyst deactivation, it is necessary to note that the type and morphology of carbon also play a significant role in determining the catalyst stability. Due to its ability to prevent reactants from reaching the metallic sites, higher levels of deactivation are often observed during cases in which encapsulating coke amounts are high. In terms of coke removal, the propensity of encapsulating coke to combust and/or gasify can be attributed to its close distance to metal sites. On the other hand, the Boudouard reaction and methane cracking give rise to the accumulation of filamentous coke, which under certain circumstances also leads to deactivation. Catalyst deactivation as a consequence of filamentous coking is characterized by a large quantity of filaments obstructing the path between reactants and catalyst pores, encapsulation of metal particles caused by the clumping and tangling of filaments, and loss of the metal active sites in the process of removing carbon filaments. In comparison to encapsulating coke, removal of filamentous carbon by gasification or combustion demands higher temperatures. This is attributed to its closer proximity to metal sites and its graphitic structure. Studies have shown that metal particle morphology can also play a role in the effects of coke formation, as larger metal particles tend to result in the formation of filamentous carbon, while smaller particles gravitate towards the production of non-filamentous carbon. In addition, catalysts of a highly porous nature are seemingly useful for preventing the decomposition of the catalyst structure and complete pore plugging due to its ability to prevent carbon filaments from forming on the metal particles.

Despite the many advances made in catalytic development, especially with activity and stability, a novel catalytic system that is both economically viable and resistant to deactivation has not yet been achieved. Most research efforts have focused on the development of catalytic materials and adjustment of properties and metal interactions for the desired catalyst activity and long-term stability. However, many aspects should be covered during the evaluation of bimetallic catalysts such as metal ratio, support, or technique of preparation to maximize the catalytic performance while also suppressing carbon accumulation. Advancement of catalyst performance for the DRM process requires consideration of the effect of operating conditions on the amount, type, and location of coke.

Future research should also consider the results of the various bimetallic studies already conducted and build upon their findings to further the objective of mitigating catalyst deactivation by carbon deposition. In particular, in situ measurements using synchrotron-based techniques, such as XAS, should be performed to understand how the local environment of bimetallic catalysts affects carbon deposition and its effective removal. In situ studies using Raman spectroscopy should also be carried out to correlate bimetallic compositions with the type of carbon generated during DRM. Systematic and in-depth DFT calculations should also be performed to determine how the formation of bimetallic catalysts affects the reaction pathways for both carbon accumulation and removal in order to design better bimetallic catalysts for the DMR reaction.

Acknowledgments
This work was supported in part by the National Science Foundation under Grant No. 1955521. Acknowledgment is made to the Donors of the American Chemical Society Petroleum Research Fund, for partial support of this work. This project was supported in part by the U.S. Department

of Energy, Office of Science, Office of Workforce Development for Teachers and Scientists (WDTS) under the Science Undergraduate Laboratory Internships Program (SULI) and Visiting Faculty Program (VFP). Work done at Brookhaven National Laboratory (BNL) was supported by the U.S. Department of Energy (DOE), grant DE-SC0012704.

References

[1] M.-E. Dias De Oliveira, B.-E. Vaughan, E.-J. Rykiel, BioSci., 55 (2005) 593–602.

[2] M.-M. Zain, A.-R. Mohammad, Renew. Sustain. Energy Rev., 98 (2018) 56–63.

[3] D.-B. Pal, R. Chand, S.-N. Upadhyay, P.-K. Mishra, Renew Sustain Energy Rev., 93 (2018) 549–565.

[4] S. Arora and R. Prasad, RSC Adv., 6 (2016) 108668.

[5] A. Abdulrasheeda, A.-A. Jalila, Y. Gamboa, M. Ibrahima, H.-U. Hambalia, M.-Y. Hamid, Renew. Sust. Energ. Rev., 108 (2019) 175–193.

[6] L.-Q.Wu, X.-J Xie, H.-L. Ren, X.-Y. Gao, Mater. Today: Proc., 42 (2021) 153–160.

[7] D.-P. Minh, X.-H. Pham, T.-J. Siang, D.V.-N. Vo, Appl. Catal. A: Gen., 621 (2021) 118202.

[8] B. Abdullah, N.A.-A. Ghani, D.V. -N. Vo, J. Clean. Prod., 162 (2017) 170e185.

[9] L.-P. Teh, H.-D. Setiabudi, S.-N. Timmiati, M.A.-A. Aziz, N.H.-R. Annuar, N.-N. Ruslan, Chem. Eng. Sci., 239 (2021) 116606.

[10] X.-Y. Wu, L.-L. Xu, M.-D. Chen, C.-F. Lv, X.-Y. Wen, Y. Cui, C. Wu, B. Yang, Z.-C. Miao and X. Hu, Front. Chem., 8 (2020) 581923.

[11] I.-V. Yentekakis, P. Panagiotopoulou, G. Artemakis, Appl. Catal. B: Environ., 296 (2021) 120210.

[12] S. Bhattar, M.-A. Abedin, S. Kanitkar, J.-J. Spivey, Catal. Today, 365 (2021) 2–23.

[13] M.-A. Ab Aziz, H.-D. Setiabudi, L.-P. The, M. Asmadi, J. Matmin, S. Wongsakulphasatch, Chem. Eng. Technol., 43 (2020) 661–671.

[14] Y. Wei, M. Song, L. Yu, F. Meng, Process Saf. Environ. Prot., 145 (2021) 236–246.

[15] N.A.-K. Aramouni, J.-G. Touma, B.-A. Tarboush, J. Zeaiter, M.N. Admad, Renew. Sustain. Energy Rev., 82 (2018) 2570–2585.

[16] J.-R. Rostrup-Nielsen, J. Sehested, J.K. Nørskov, Adv. Catal., 47 (2002) 65–139.

[17] C. Papadopoulou, H. Matralis, X. Verykios, Catalysis for alternative energy generation. Springer Nature (2012) 57–127.

[18] G.A. Somorjai, Y.M. Li, Introduction to Surface Chemistry and Catalysis (2nd edition), John Wiley & Sons, Inc., Hoboken, New Jersey, 2010, pp. 443—464.

[19] R. Juarez-Mosqueda, A. Mavrandonakis, A.-B. Kuc, L.G.-M. Pettersson, T. Heine, Front. Chem., 3 (2015) 1–9.

[20] M.C.-J. Bradford, M.-A. Vannice, Appl. Catal. A: Gen., 142 (1996) 97–122.

[21] P.-M. Mortensen, I. Dybkjær, Appl. Catal. A: Gen., 495 (2015) 141–151.

[22] U. Olsbye, T. Wurzel, L. Mleczko, Ind. Eng. Chem. Res., 36 (1997) 5180–5188.

[23] A.-J. Brungs, A.P.-E. York, J.-B. Claridge, C. Márquez-Alvarez, Catal. Lett., 70 (2000) 117–122.

[24] S.-C. Tsang, J.-B. Claridge, M.L.-H. Green, Catal. Today, 23 (1995) 3–15.

[25] S. Wang, G.-Q. Lu, G.-J. Millar, Energy Fuels, 10 (1996) 896–904.

[26] J. Zhang, H. Wang, A.-K. Dalai, J. Catal., 249 (2007) 300–310.

[27] D. San-José-Alonso, J. Juan-Juan, M.-J. Illán-Gómez, M.-C Román-Martínez, Appl. Catal. A: Gen., 371 (2009) 54–59.

[28] A.-M. Gadalla, B. Bower, Chem. Eng. Sci., 43 (1988) 3049–3062.

[29] M.-K. Nikoo, N.A.-S. Amin, Fuel Proc. Tech., 92 (2011) 678–691.

[30] D. Pakhare, J. Spivey, Chem. Soc. Rev., 43 (2014) 7813–7837

[31] L.C.-S. Kahle, T. Roussière, L. Maier, K.-H. Delgado, G. Wasserschaff, S.-A. Schunk, O. Deutschmann, Ind. Eng. Chem. Res., 52 (2013) 11920–11930.

[32] A.-A. Abdulrasheed, A.-A. Jalil, T.-J. Siang, H.-U. Hambali, IOP Conf. Ser.: Mater. Sci. Eng., 808 (2020) 012001.

[33] N.A.-K. Aramouni, J. Zeaiter, W. Kwapinski, M.-N. Ahmad, Energy Conv. Man., 150 (2017) 614–622.

[34] R.-Y. Chein, Y.-C. Chen, C.-T. Yu, J.-N. Chung, J. Nat. Gas. Sci. Eng., 26 (2015) 617–629.

[35] A. Tsoukalou, Q. Imtiaz, S.-M. Kim, P.-M. Abdala, S. Yoon, C.-R. Müller, J. Catal., 343 (2016) 208–214.

[36] D. Zambrano, J. Soler, J. Herguido, M. Menéndez, Top. Catal., 62 (2019) 456–466.

[37] J. Wei and E. Iglesia, J. Catal., 224 (2004) 370–383.

[38] J. Wei and E. Iglesia, J. Phys. Chem. B, 108 (2004) 4094–4103.

[39] J. Wei and E. Iglesia, Phys. Chem. Chem. Phys., 6 (2004) 3754–3759.

[40] J. Wei and E. Iglesia, J. Catal., 225 (2004) 116–127.

[41] C., Crisafulli, S. Scire, S. Minico and L. Solarina, Appl. Catal. A: Gen., 225 (2002) 1–9.

[42] A.S.-A. Al-Fatesh, A.-H. Fakeeha and A.-E. Abasaeed, Chin. J. Catal., 32 (2011) 1604–1609.

[43] A. Horvath, G. Stefler, O. Geszti, A. Kienneman, A. Pietraszek and L. Gucai, Catal. Today, 169 (2011) 102–111.

[44] M. Ghelamallah and P. Granger, Appl. Catal. A: Gen., 485 (2015) 172–180.

[45] M. García-Diéguez, E. Finocchio, M.-A. Larrubia, L.-J. Alemany and G. Busca, J. Catal., 274 (2010) 11–20.

[46] N. Tsubaki, S. Sun and K. Fujimoto, J. Catal., 199 (2001) 236–246.

[47] J. Zhang, H. Wang, A. Dalai, J. Catal., 249 (2007) 300–310.

[48] T.-S. Phan, A.-R. Sane, B. Rêgo de Vasconcelos, A. Nzihou, P. Sharrock, D. Grouset, D. Pham Minh, Appl. Catal B: Environ., 224 (2018) 310–321.

[49] F. Wang, L.-L. Xu, J. Yang, J. Zhang, L.-Z. Zhang, H. Li, Y. Zhao, H.-X. Li, K. Wu, G. -Q. Xu, W. Chen, Catal. Today, 281 (2017) 295–303.

[50] Z.-F. Bian, S. Das, M.-H. Wai, P. Hongmanorom, S. Kawi, Chem. Phys. Chem., 18 (2017) 3117–3134

[51] L. Foppa, M.-C. Silaghi, K. Larmier, A. Comas-Vives, J. Catal., 343 (2016) 196–207.
[52] K. Tomishige. Catal. Today, 89 (2004) 405–418.

[53] L.-D. Li, L. Zhou, S. Ould-Chikh, D.-H. Anjum, M.-B. Kanoun, J. Scaranto, M.-N. Hedhili, S. Khalid, P.-V. Laveille, L. D'Souza, A. Clo, J.-M. Basset, ChemCatChem, 7 (2015) 819–829.

[54] Z.-Y. Hou, P. Chen, H.-L. Fang, X.-M. Zheng, T. Yashima, Int. J. Hydrog. Energy, 31 (2006) 555–561.

[55] A. Tsyganok, Catal. Commun., 4 (2003) 493–498.

[56] S.-A. Theofanidis, V.-V. Galvita, H. Poelman, G.-B. Marin, ACS Catal., 5 (2015) 3028–3039.

[57] U. Guharoy, E. Le Saché, Q. Cai, T.-R. Reina and S. Gu, J. CO_2 Util., 27 (2018) 1–10.

[58] H. Arandiyan, Y. Peng, C. Liu, H. Chang and J. Li. J. CO_2 Util., 89 (2013) 372–381.

[59] D. Liu, X.-Y. Quek, W.N.-E. Cheo, R. Lau, A. Borgna and Y. Yang, J. Catal., 266 (2009) 380–390.

[60] N. El Hassan, M.-N. Kaydouh, H. Geagea, H. El Zein, K. Jabbour, S. Casale, H. Zakhem and P. Massiani, Appl. Catal. A: Gen., 520 (2016) 114–121.

[61] X. Fan, Z. Liu., Y.-A. Zhu, G. Tong, J. Zhang, C. Egelbrekt, J. Ulstrup, K. Zhu and X. Zhou, J. Catal., 330 (2010) 106–119.

[62] Z. Jiang, X. Liao and Y. Zhao, Appl. Petrochem. Res., 3 (2013) 91–99.

[63] Z. Alipour, M. Rezaei and F. Meshkani, J. Ind. Eng. Chem., 20 (2014) 2858–2863.

[64] W.-J. Jang, D.W. zjeong, J.-O. Shim, H.-S. Roh, I.-H. Son and S.-J. Lee, Int. J. Hydrog. Energy, 38 (2013) 4508–4512.

[65] R. L. Mieville, J. Catal., 100 (1986) 482–488.

[66] R.-L. Mieville, Stud. Surf. Sci. Catal., 68 (1991) 151–159.

[67] M. Guisnet, P. Magnoux, Appl. Catal. A: Gen., 212 (2001) 83–96.

[68] F. Goettmann, C. Sanchez, J. Mat. Chem., 17 (2007) 24–30.

[69] F. Barrai, T. Jackson, N. Whitmore, M. J. Castaldi, Catal. Today, 129 (2007 391–396.

[70] N.A.-K. Aramouni, J. Zeaiter, W. Kwapinski, J.-J. Leahy, M.-N. Ahmad, J. CO_2 Util., 44 (2021) 101411–101424.

[71] D. Duprez, M.-C. DeMicheli, P. Marecot, J. Barbier, O. A. Ferretti, E.-N. Ponzi, J. Catal., 124 (1990) 324–335.

[72] C.-T. Campbell, S.-C. Parker, D.-E. Starr, Science, 298 (2002) 811–814.

[73] C.-H. Bartholomew, Catal. Rev. Sci. Eng., 24 (1982) 67–112.

[74] F. Jalid, M.-A. Haider, M.-I. Alam, T.-S. Khan, Catal. Sci. Technol., 11 (2021) 2130–2143.

[75] S. Arora, R. Prasad, RSC Adv., 6 (2016) 108668–108688.

[76] A. Ochoa, J. Bilbao, A.-G. Gayubo, P. Castaño, Renew. Sus. Energy Rev., 119 (2020) 109600.

[77] M.-D. Argyle, C.-H. Bartholomew, Catalysts, 5 (2015) 145–269.

[78] X. Zhao, B. Joseph, J. Kuhn, S. Ozcan, iScience, 23 (2020) 101082.

[79] J.-R. Rostrup-Nielsen and P.-B. Tottrup, Proc. Symp. Sci. Catal. Its Appl. Indus., FPDIL, Sindri, India, 1979, p. 379.

[80] J.-R. Rostrup-Nielsen, in: J.-R. Anderson, M. Boudart (eds), Catalysis, Science and Technology, Springer, Berlin, Heidelberg, 1984, pp. 1–117.

[81] J.-R. Rostrup-Nielsen, Chem. Eng. Prog., 73 (1977) 87.

[82] F. Moseley, R.-W. Stephens, K.-D. Stewart and J. Wood, J. Catal., 24 (1972) 18–39.

[83] J. Lahaye, P. Badie, J. Ducret, Carbon, 15 (1977) 87–93.

[84] I. Alstrup. J. Catal., 109 (1988) 241–251.

[85] I. Alstrup, M.-T. Tavaes, C.-A. Bernardo, O. Sorensen and J.-R. Rostrup-Nielsen, Mater. Corros., 49 (1998) 367–372.

[86] R.T.-K. Baker, M.-A. Barber, P.-S. Harris, F.-S. Feates, R.-J. Waite, J. Catal., 26 (1972) 51–62.

[87] T. Borowiecki, Appl. Catal., 4 (1982) 223–231.

[88] S. Helveg, J. Sehested and J.-R. Rostrup-Nielsen, Catal. Today, 178 (2011) 42–46.

[89] S. Helveg, C. Lo´pez-Cartes, J. Sehested, P.-L. Hansen, B.-S. Clausen, J.-R. Rostrup-Nielsen, F. Abild-Pedersen and J.-K. Nørskov, Nature, 427, (2004) 426–429.

[90] F. Abild-Pedersen and J.-K. Nørskov, Phys. Rev. B, 73 (2006) 115419.

[91] J.-R. Rostrup-Nielsen, Catal. Today, 63 (2000) 159–64.

[92] J.-M. Ginsburg, J. Piña, T. El Solh, H.-I. de Lasa, Ind. Eng. Chem. Res,, 44 (2005) 4846–4854.

[93] R.T.-K. Baker, M.-A. Barber, P.-S. Harris, F.-S. Feates, R.-J. Waite, J. Catal., 26 (1972) 51–62.

[94] F. Abild-Pedersen, J.-K. Nørskov, J.-R. Rostrup-Nielsen, J. Sehested, S. Helveg, Phys. Rev. B., 73 (2006) 115419.

[95] J.-R. Rostrup-Nielsen, D.-L. Trimm, J. Catal., 48 (1977) 155–165.

[96] T. Saelee, M. Lerdpongsiripaisarn, M. Rittiruam, S. Somdee, A. Liu, S. Praserthdam, P. Praserthdam, Sci Rep., 11 (2021) 519.

[97] J. Yoo, Y. Bang, S.-J. Han, S. Park, J.-H. Song, I.-K. Song, J. Mol. Catal. A: Chem., 410 (2015) 74–80.

[98] A.-M. Molenbroek and J.-K. Nørskov, J. Phys. Chem. B, 105 (2001) 5450–5458.

[99] F. Besenbacher, I. Chorkendorff, B.-S. Clausen, B. Hammer, A.M. Molenbroek, J.K. Nørskov and I. Stensgaard, Science, 279 (1998) 1913.

[100] J.-R. Rostrup-Nielsen and J.-K. Nørskov, Top. Catal. 40 (2006) 1–4.

[101] E. Nikolla, A. Holewinski, J. Schwank, S. Linic, J. Am. Chem. Soc., 128 (2006) 11354–11355.

[102] H.-S. Bengaard, J.-K. Nørskova, J. Sehested, B.-S. Clausen, L.-P. Nielsen, A.-M. Molenbroek, J.-R. Rostrup-Nielsen, J. Catal., 209 (2002) 365–384.

[103] A. Abdulrasheed, A.-A. Jalil, Y. Gambo, M. Ibrahim, H.-U. Hambali, M.Y.-S. Hamid, Renew. Sustain. Energy Rev., 108 (2019) 175–193.

[104] H. Li, K. Shin, G. Henkelman, J. Chem. Phys., 149 (2018) 174705.

[105] J.-R. Kitchin, J.-K. Nørskov, M.-A. Barteau, J.-G. Chen, Phys. Rev. Lett., 93 (2004) 156801.

[106] W. Yu, M.-D. Porosoff, J.-G. Chen, Chem. Rev., 112 (2012) 5780–5817.

[107] D.-Y. Jo, M.-W. Lee, C.-H. Kim, J.-W. Choung, H.-C. Ham, K.-Y. Lee, Catal. Today, 359 (2021) 57–64.

[108] W. Jang, J. Shim, H. Kim, S. Yoo, H. Roh, Catal. Today, 324 (2019) 15–26.

[109] Z. Bao, F. Yu, Adv. Bioener., 3 (2018) 43–76.

[110] A. Al-Fatesh, J. King Saud Univ. Eng. Sci., 27 (2015) 101–107.

[111] T.-J. Siang, S. Singh, O. Omoregbe, L.-G. Bach, N.H.H. Phuc, D.-N. Vo, J. Energy Inst., 91 (2018) 683–694.

[112] T.-S. Phan, A.-R. Sane, B.-R. de Vasconcelos, A. Nzihou, P. Sharrock, D. Grouset, D.-P. Minh, Appl. Catal. B: Environ., 224 (2018) 310–321.

[113] Y. Turap, I. Wang, T. Fu, Y. Wu, Y. Wang, W. Wang, Int. J. Hydrog. Energy, 45 (2020) 6538–6548.

[114] J. Zhang, H. Wang, A.-K. Dalai, Appl. Catal. A: Gen., 339 (2008) 121–129.

[115] R. Ferrando, J. Jellinek, R.-L. Johnston, Chem. Rev., 108 (2008) 845–910.

[116] Luisetto, S. Tuti, E. Di Bartolomeo, Int. J. Hydrog. Energy, 37 (2012) 15992–15999.

[117] M.-S. Fan, A.-Z. Abdullah, S. Bhatia, Appl Catal B: Environ., 100 (2010) 365–377.

[118] K. Takanabe, K. Nagaoka, K. Nariai, K. Aika, J. Catal., 232 (2005) 268–275.

[119] B. Erdogan, H. Arbag, N. Yasyerli, Int. J. Hydrog. Energy, 48 (2018) 1396–1405.

[120] B. AlSabban, L. Falivene, S.-M. Kozlov, A. Aguilar-Tapia, S. Ould-Chikh, J.-L. Hazemann, L. Cavallo, J.M. Basset, K. Takanabe, Appl. Catal. B: Env., 213 (2017) 177–189.

[121] K.Takanabe, K. Nagaoka, K. Aika, Catal. Lett., 102 (2005) 153–157.

[122] J. Xin, H. Cui, Z. Cheng, Z. Zhou, Appl. Catal. A, Gen., 554 (2018) 95–104.

[123] H. Wu, J. Liu, H. Liu, D. He, Fuel, 235 (2019) 868–77.

[124] J. Horlyck, C. Lawrey, E.-C. Lovell, R. Amal, J. Scott, Chem. Eng. J., 352 (2018) 572–580.

[125] K. Sheng, D. Luan, H. Jiang, F. Zeng, B. Wei, F. Pang, J. Ge, ACS Appl. Mater. Interfaces, 11 (2019) 24078–24087.

[126] W. Tu, M. Ghoussoub, C.-V. Singh, Y.H.-C. Chin, J. Am. Chem. Soc., 139 (2017) 6928–6945.

[127] Z. Bian, S. Das, M.H. Wai, P. Hongmanorom, S. Kawi, ChemPhysChem, 18 (2017) 3117–3134.

[128] W. Liu, L. Li, S. Lin, Y, Luo, Z. Bao, Y. Mao, K. Li, D. Wu, H. Peng, J. Energy Chem. 65 (2022) 34–47.

[129] C. Wan, K. Song, J. Pan, M. Huang, R. Luo, D. Li, L. Jiang, Int. J. Hydrog. Energy, 45 (2020) 33574–33585.

[130] M. Yusuf, A.S. Farooqi, A.-A. Al-Kahtani, M. Ubaidullah, M.-A. Alam, L.-K. Keong, K. Hellgardt, B. Abdullah, Int. J. Hydrog. Energy, 2021, in press.

[131] U. Guharoy, E. Le Saché, Q. Cai, T.-R. Reina, S. Gu, J. CO_2 Util., 27 (2018) 1–10.

[132] H.-S. Bengaard, J.-K. NØrskov, J. Sehested, B.-S. Clausen, L.-P. Nielsen, A.-M. Molenbroek, J.R. Rostrup-Nielsen, J. Catal., 209 (2002) 265–384.

[133] Y. Song, E. Ozdemir, S. Ramesh, A. Adishev, S. Subramanian, A. Harale, M. Albuali, B.-A. Fadhel, A. Jamal, D. Moon, S.-H. Choi, C.-T. Yavuz, Science. 367 (2020) 777–781.

[134] L. Dehimi, M. Gaillard, M. Virginie, A. Erto, Y. Benguerba, Int. J. Hydrog. Energy, 45 (2020) 24657–24669.

[135] J. Guo, H. Lou, H. Zhao, D. Chai, X. Zheng, Appl. Catal. A: Gen., 273 (2004) 75–82.

[136] T. Huang, W. Huang, J. Huang, P. Ji, Fuel Proc. Tech., 92 (2011) 1868–1875.

[137] F.-R. Shamskar, F. Meshkani, M. Rezaei, J. CO_2. Util., 22 (2017) 124–134.

[138] R. de, S. Monteiro, F.-B. Noronha, L.-C. Dieguez, M. Schmal, Appl. Catal. A: Gen., 131 (1995) 89–106.

[139] R. Yang, C. Xing, C. Lv, L. Shi, N. Tsubaki, Appl. Catal. A: Gen., 385 (2010) 92–100.

[140] R.-Y. Chein, W.-Y. Fung, Int. J. Hydrog. Energy, 44 (2019) 14303–14315.

[141] R.-K. Singha, A. Shukla, A. Yadav, T. Sasaki, A. Sandupatla, G. Deo, R. Bal, Catal. Sci. Tech., 7 (2017) 4720–4735.

[142] D. Liu, X.-Y. Quek, W.N.-E. Cheo, R. Lau, A. Borgna, Y. Yang, J. Catal., 266 (2009) 380–390.

[143] Y. Lu, L. Kang, D. Guo, Y. Zhao, Y. Zhao, S. Wang, X. Ma, ACS Catal., 11 (2021) 8749–8765.

[144] S.-A. Theofanidis, V.-V. Galvita, H. Poelman, G.-B. Marin, ACS Catal., 5 (2015) 3028–3039.

[145] I.-V. Yentekakis, P. Panagiotopoulou, G. Artemakis, Appl. Catal. B: Environ. 296 (2021) 120210–120251.

[146] H. Qiu, J. Ran, J. Niu, F. Guo, Z. Ou, Mol. Catal., 502 (2021) 111360.

[147] A. Omran, S.-H. Yoon, M. Khan, M. Ghouri, A. Chatla, N. Elbashir, Catalysts 10 (2020) 1043–1060.

[148] J.-S. Chang, S.-E. Park, H. Chon, Appl Catal. A: Gen., 145 (1996) 111–124.

[149] C. Pan, Z. Guo, H. Dai, R. Ren, W. Chu, Int. J. Hydrog. Energy, 45 (2020) 16133–16143.

[150] B. Steinhauer, M.-R. Kasireddy, J. Radnik, A. Martin, Appl. Catal. A: Gen., 366 (2009) 333–341.

[151] D.-G. Araiza, D.-G. Arcos, A. Gómez-Cortés, G. Díaz, Catal. Today, 360 (2021) 46–54.

[152] F. Meshkani, M. Rezaei, Int. J. Hydrog. Energy, 35 (2010) 10295–10301.

[153] L. Li, L. Zhou, S. Ould-Chikh, D.-H. Anjum, M.-B. Kanoun, J. Scaranto, M.-N. Hedhili, S. Khalid, P.V. Laveille, L. D'Souza, A. Clo, J. Basset, ChemCatChem, 7 (2015) 819–829.

[154] A.-I. Tsyganok, M. Inaba, T. Tsunoda, K. Uchida, K. Suzuki, K. Takehira, T. Hayakawa, Appl. Catal. A: Gen., 292 (2005) 328–343.

[155] R. Mahfouz, J. Estephane, C. Gennequin, L. Tidahy, S. Aouad, E. Abi-Aad, J. Chem. Eng., 9 (2021) 104662–104671.

[156] C. Crisafulli, S. Scirè, S. Minicò, L. Solarino, Appl. Catal. A: Gen., 225 (2002) 1–9.

[157] S. Andraos, R. Abbas-Ghaleb, D. Chala, A. Vita, C. Italiano, M. Laganà, Int. J. Hydrog. Energy, 44 (2019) 25706–25716.

[158] A. Álvarez M, L.-F. Bobadilla, V. Garcilaso, M.-A. Centeno, J.A. Odriozola, J. CO_2 Util., 24 (2018) 509–515.

[159] T. Mozammel, D. Dumbre, R. Hubesch, G.-D. Yadav, P.-R. Selvakannan, S.-K. Bhargava, Energy Fuels, 34 (2020) 16433–16444.

[160] S. Özkara-Aydinoğlu, A.-E. Aksoylu, Catal. Commun., 11 (2010) 1165–1170.

[161] A.-I. Paksoy, B.-S. Caglayan, A.-E. Aksoylu, Appl. Catal. B: Environ., 168-169 (2015) 164–174.

[162] Y. Pang, Y. Dou, A. Zhong, W. Jiang, L. Gu, X. Feng, W. Ji, C. Au, Appl. Catal. A: Gen., 555 (2018) 27–35.

[163] N. El Hassan, M.-N. Kaydouth, H. Geagea, H. El Zein, K. Jabbour, S. Casale, H. El Zakhem, P. Massiani, Appl. Catal. A: Gen., 520 (2016) 114–121.

[164] Z. Xie, B. Yan, S. Kattel, J.-H. Lee, S. Yao, Q. Wu, N. Rui, E. Gomez, Z. Liu, W. Xu, L. Zhang, J.-G. Chen, Appl. Catal. B: Environ., 236 (2018) 280–293.

[165] K. Nagaoka, K. Takanabe, K. Aika, Appl. Catal. A: Gen., 268 (2004) 151–158.

[166] A. Jawad, F. Rezaei, A.-A. Rownaghi, Catal. Today, 350 (2020) 80–90.

[167] X. Fu, H. Su, W. Yin, Y. Huang, X. Gu, Catal. Sci. Technol., 7 (2017) 1671–1678

[168] H.-M. Nguyen, G.-H. Pham, M. Tade, C. Phan, R. Vagnoni, S. Liu, Energy Fuels, 34 (2020) 7284–7294.

Graphical Abstract

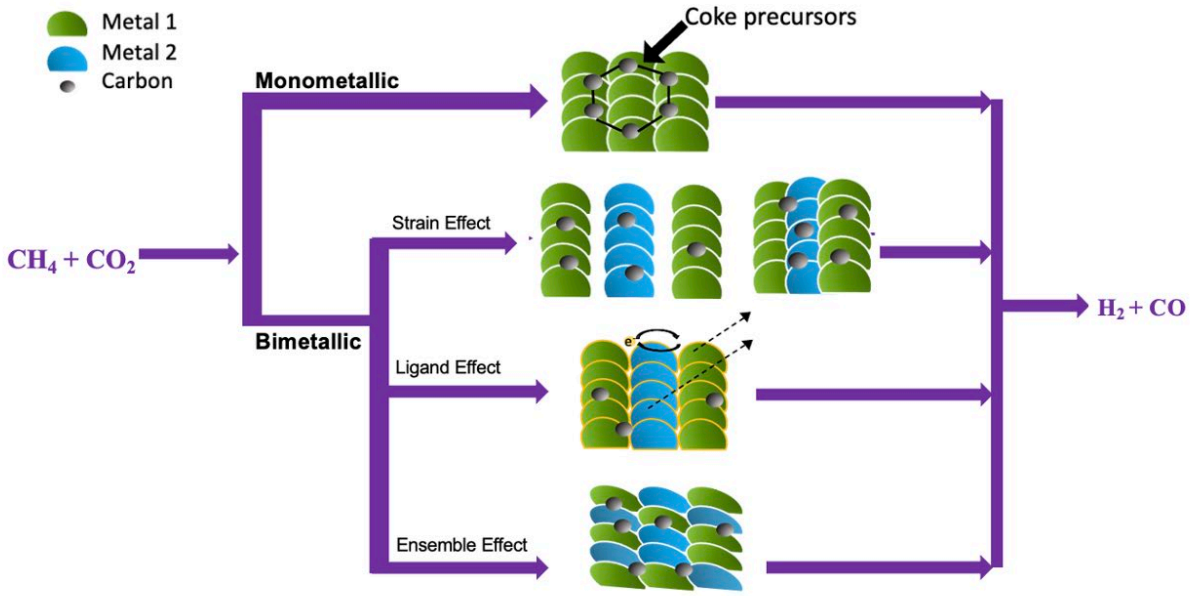

Bimetallic catalysts can potentially reduce coke deposition due to ligand, strain and ensemble effects. This article reviews utilization of bimetallic catalysts to mitigate coke formation in dry reforming of methane.